COMPACT WAVEGUIDE GRATING COUPLERS OPERATING IN THE STRONG COUPLING REGIME

by

BIN WANG

A DISSERTATION

Submitted in partial fulfillment of the requirements
for the degree of Doctor of Philosophy
in
The Optical Science and Engineering Program
to
The School of Graduate Studies
of
The University of Alabama in Huntsville

HUNTSVILLE, ALABAMA

2005

In presenting this dissertation in partial fulfillment of the requirements for a doctoral degree from The University of Alabama in Huntsville, I agree that the Library of this University shall make it freely available for inspection. I further agree that permission for extensive copying for scholarly purposes may be granted by my advisor or, in his/her absence, by the Director of the Program or the Dean of the School of Graduate Studies. It is also understood that due recognition shall be given to me and to The University of Alabama in Huntsville in any scholarly use which may be made of any material in this dissertation.

_____ _____

(student signature) (date)

DISSERTATION APPROVAL FORM

Submitted by Bin Wang in partial fulfillment of the requirements for the degree of Doctor of Philosophy in Optical Science and Engineering and accepted on behalf of the Faculty of the School of Graduate Studies by the dissertation committee.

We, the undersigned members of the Graduate Faculty of The University of Alabama in Huntsville, certify that we have advised and/or supervised the candidate on the work described in this dissertation. We further certify that we have reviewed the dissertation manuscript and approve it in partial fulfillment of the requirements of the degree of Doctor of Philosophy in Optical Science & Engineering.

_____ Committee Chair

_____

_____

_____

_____

_____

_____ Program Director

_____ College Dean

_____ Graduate Dean

ABSTRACT
School of Graduate Studies
The University of Alabama in Huntsville

Degree Doctor of Philosophy Program Optical Science and Engineering

Name of Candidate Bin Wang

Title Compact Waveguide Grating Couplers Operating in the Strong Coupling Regime

Since both photonic crystal and high index contrast waveguide photonic devices allow for tighter bend radii and thus reduced die size, they are being actively investigated for use in dense planar lightwave circuits (PLCs). To fully realize highly integrated PLCs, an efficient optical connection interface between single mode fibers or fiber arrays and high-index-contrast waveguides is required. The core size of single-mode fiber is typically 4-9μm while the core size of high-index-contrast waveguides is usually less than 1 to 2μm. Due to the mode size mismatch between the fiber and the waveguide, coupling light into small waveguides is challenging. This results in prohibitive insertion loss and extreme difficulty in fiber alignment for simple pigtail coupling, in which the end of a fiber is aligned and placed next to the end face of a waveguide. In addition, with input and output coupling taking place only along the edge of a chip at the plane of the waveguide device layer, this edge coupling arrangement severely limits the number of optical I/Os in dense PLCs. Moreover, fiber alignment has to be done after the wafer is

diced into separate chips, and the end facet of the waveguide needs to be cut and polished. As a result, alignment and packaging accounts for the main manufacturing cost of optical components. In order to fully realize the potential of highly integrated PLCs, a new coupling approach needs to be developed, especially one that permits input and output to a 2-D array of fibers.

The goal of this dissertation is to develop a high efficiency coupling method based on grating couplers operating in the strong coupling regime for fibers oriented normal to the waveguide plane without any intermediate optics between the fibers and waveguides. Development of this capability allows for relaxed fiber alignment requirements and wafer-scale alignment and testing.

In this dissertation, three types of grating couplers that operate in the strong coupling regime are investigated. These are (1) stratified waveguide grating couplers (SWGCs), (2) slanted grating couplers (SLGCs) and (3) embedded slanted grating couplers (ESGCs). With the use of micro genetic algorithm (μGA) in conjunction with the finite difference time domain method, specific designs based on different high index contrast waveguides are presented. A simplified k-vector diagram together with the rigorous coupled wave analysis (RCWA) mode solver method have been suggested and explored in order to analyze and understand the physical principles of strong grating couplers. On the basis of this understanding, a systematic design procedure for uniform slanted grating couplers is developed and shown to be effective. This design procedure avoids the computational requirements needed for a purely numerical design based on the μGA method.

Abstract Approval: Committee Chair _____
(Date)

Department Chair _____

Graduate Dean _____

ACKNOWLEDGMENTS

The work presented in this dissertation would not have been possible without the assistance of many people. First, I would like to thank my advisor, Dr. G. P. Nordin, for his suggestion for the research topic, and his guidance and encouragement through the entire research process. I also thank my committee members, Dr. Robert Lindquist, Dr. Lloyd Hillman, Dr. Patrick Reardon, Dr. Joseph Geary and Dr. Jamshid Nayyer, for serving on my committee, and Dr. Don Gregory for reviewing this manuscript. Special thanks go to Dr. Jianhua Jiang for his concrete support in codes modification, many enlightening conversations and help in writing journal papers. I would like to express my appreciation to Dr. Frank Madarasz for his help in correcting my English in this dissertation.

I also would like to give my thanks to Dr. Seunghyun Kim, Dr. Jingbo Cai; graduate students, Ashwini and Jaime; staff, Linda and Judy in the Nano and Micro Devices Center. They were always nice and helpful during my study.

Finally, I would like to thank my husband, Hua, for always encouraging and supporting me working on this degree. My dear son, Eric, born during my study at UAH, brings me happiness every day in my life. Gratefulness is also given to my parents and parents-in-law who provided much help which enabled me to complete this work.

TABLE OF CONTENTS

Page

LIST OF FIGURES xi

LIST OF TABLES xvi

LIST OF SYMBOLS xvii

LIST OF ACRONYMS xix

CHAPTER

1 INTRODUCTION 1

1.1 Motivation 1

1.2 Overview of the dissertation 3

1.3 New contributions 6

2 BACKGROUND 8

2.1 Coupling between high index contrast waveguides and single mode fibers 8

2.2 Most widely researched and used methods 10

2.3 Vertical fiber coupling and grating coupler 12

2.4 Research review for vertical fiber coupling 15

2.5 Computational tools 16

2.5.1 Two-dimensional Finite difference time domain (2-D FDTD) Method 16

2.5.2 Micro genetic algorithm (μGA) with 2-D FDTD 20

2.5.3 Rigorous Coupled-Wave Analysis (RCWA) mode solver and reflectance calculation for grating structures with any profile 21

3 STRATIFIED WAVEGUIDE GRATING COUPLER FOR NORMAL FIBER INCIDENCE 23
3.1 Strong grating coupler for vertical fiber coupling 24
3.2 Design and simulation 26
3.3 Physical analysis and discussion 32
3.4 Fabrication tolerance 37
3.5 Conclusions 37
4 COMPACT SLANTED WAVEGUIDE GRATING COUPLER 38
4.1 Motivation 38
4.2 SLGC simulation and design 40
4.2.1 Uniform SLGC 42
4.2.2 Non-uniform SLGC 44
4.3 Physical analysis and discussion 47
4.4 Fabrication tolerance 54
4.5 Output coupler 54
4.6 Conclusions 59
5 EMBEDDED SLANTED GRATING 61
5.1 Introduction 61
5.2 ESGC simulation and design based on SOI waveguide 62
5.2.1 Simulation results 62
5.2.2 Discussion 69
5.2.3 Fabrication and alignment tolerance 72
5.3 ESGC simulation and design based on polymer waveguide 72

5.4 Conclusions 77
6 SYSTEMATIC DESIGN PROCESS FOR UNIFORM SLANTED GRATING COUPLER AT BRAGG ANGLE 78
6.1 Design process 78
6.2 Design example based on SOI waveguide 81
6.2.1 Fill factor of 0.328 82
6.2.2 Fill factor of 0.5 84
6.3 Conclusions 87
7 DISCUSSION AND CONCLUSIONS 88
7.1 Summary 88
7.2 Future research 91
7.2.1 3-D analysis and evaluation 92
7.2.2 Fabrication of stratified and slanted grating structures 92
REFERENCES 94

LIST OF FIGURES

Figure		Page
2.1	Pigtail coupling.	9
2.2	Sketch of vertical fiber coupling arrangement.	12
2.3	Vertical fiber coupling arrangement with (a) symmetric binary grating. (b) asymmetric grating.	13
2.4	Vertical fiber coupling arrangement proposed by Taillaert et al. (IEEE Journal of Quantum Electronics, Vol.38, No.7, July 2002).	16
2.5	Position of the electric and magnetic field vector components about 2-D unit cell of the Yee space lattice for TE polarization calculation.	19
3.1	3D geometry of the strong grating coupler for normal coupling between fiber and waveguide.	24
3.2	SWGC geometry for FDTD simulation.	26
3.3	The μGA FDTD optimized result of magnitude squared time averaged E_z component with single binary grating layer.	29
3.4	The μGA FDTD optimized result of magnitude squared time averaged E_z component with double binary grating layer.	29
3.5	Magnitude time averaged electric field calculated with 2-D FDTD.	31
3.6	K-vector diagram of SWGC.	34
3.7	(a) Spectral response of the SWGC. (b) Lateral shift sensitivity analysis of the SWGC based on a fiber lateral shift as in Figure 3.5.	36

4.1 SEM picture of preliminary etching result of deep slanted grating using Atomic Oxygen Etching technique on polyimide material at Los Alamos National Laboratory [55]. 39

4.2 2D cross-sectional geometry of SLGC used in the 2D FDTD simulation. 41

4.3 (a) Geometry of uniform SLGC optimized by μGA. (b) 2D FDTD result of magnitude squared time averaged E_z component for the uniform SLGC. 44

4.4 (a) Geometry of non-uniform SLGC optimized by μGA. (b) 2D FDTD result of magnitude squared time averaged E_z component for the non-uniform SLGC. 45

4.5 Fill factor distribution of μGA optimized grating along x direction for non-uniform SLGC shown in Figure 4.4. 46

4.6 Infinite periodic version of the SLGC for leaky mode calculation with RCWA approach. 47

4.7 k-vector diagram of the uniform fill-factor SLGC presented in Section 4.2.1, the inset shows the slanted grating. 50

4.8. Phase distribution from 2D FDTD simulation on the uniform SLGC..... 51

4.9 (a) k-vector diagram of non-uniform SLGC. (b) 2D FDTD Phase distribution of the non-uniform SLGC. 52

4.10 2D FDTD simulated spectral response of the non-uniform SLGC design. 53

4.11 Fiber lateral shift sensitivity analysis of the non-uniform SLGC design. 53

4.12 (a) Image plot of magnitude time averaged E_z components from FDTD simulation of the uniform SLGC as an output coupler. 56

4.12 Continue (b) Phase distribution from FDTD simulation of the uniform SLGC as an output coupler. 57

4.13 (a) Image plot of magnitude time averaged E_z components from FDTD simulation of the non-uniform SLGC as an output coupler. 57

4.13 Continue (b) Phase distribution from FDTD simulation of the non-uniform SLGC as an output coupler. 58

4.14 A cross section of the near field amplitude of (a) the uniform output coupler. For comparison, the profile of fiber mode is overlapped on the plots as a dotted line. 58

4.14 Continue of (b) the non-uniform output coupler. For comparison, the profile of fiber mode is overlapped on the plots as a dotted line. 59

5.1 Schematic diagram of ESGC geometry. 63

5.2 Image plot of magnitude squared time averaged E_z component from the FDTD simulation for the uniform ESGC with a fiber having a core size of 8.3μm. 64

5.3 (a) Image plot of magnitude time averaged E_z component from the FDTD simulation when the input coupler in Figure 5.2 is used as an output coupler. (b) Cross section profile of near field of the output beam in Figure 5.3(a) with fiber mode profile (the dotted line) for comparison. The vertical dashed line shows the grating boundary at the right side. 65

5.4 Image plot of magnitude squared time averaged E_z component from FDTD simulation on the uniform ESGC for a fiber with a core size of 4.4μm. 66

5.5 (a) Image plot of the magnitude squared time averaged electric field simulated by 2D FDTD for a fiber with a core size of 4.4μm. (b) Fill factor distribution of the non-uniform ESGC in (a). 67

5.6 2D FDTD simulated spectral response of the non-uniform ESGC design. 68

5.7 k-vector diagram of ESGC. 70

5.8 The reflectivity of the optimized structure calculated by RCWA. 71

5.9 (a) Geometry of uniform ESGC based on polymer waveguide optimized by μGA. (b) 2D FDTD result of magnitude squared time averaged E_z component for the uniform ESGC. 73

5.10 (a) Geometry of non-uniform ESGC based on polymer waveguide optimized by μGA. (b) 2D FDTD result of magnitude squared time averaged E_z component for the non-uniform ESGC. (c) Fill factor distribution of the non-uniform ESGC 2D FDTD result of magnitude squared time averaged E_z in (a). 74

5.11 (a) Geometry of uniform ESGC based on polymer waveguide optimized by μGA. (b) 2D FDTD result of the magnitude squared time averaged E_z component for the uniform ESGC. 75

5.12 (a) Geometry of non-uniform ESGC based on polymer waveguide optimized by μGA. (b) 2D FDTD result of the magnitude squared time averaged E_z component for the non-uniform ESGC. (c) Fill factor distribution of the the non-uniform ESGC 2D FDTD result of magnitude squared time averaged E_z in (a). 76

6.1 2D FDTD result of the magnitude time averaged E_z component of output coupler. 82

6.2. (a) Cross section of the near field pattern of Figure 6.1. (b) Cross section of the fiber mode. 83

6.3 2D FDTD result of magnitude squared time averaged Ez component of input coupler with f=0.328. 84

6.4 (a) 2D FDTD result of magnitude time averaged E_z component for the output coupler. 85

6.4 Continue (b) Cross section of the near field pattern in (a). 86

6.5 2D FDTD result of magnitude squared time averaged Ez component of input coupler with f=0.5. 86

LIST OF TABLES

Figure Page

3.1 Structural parameters for SWGC with three grating layers.....30

4.1 μGA optimization of a uniform SLGC.....43

LIST OF SYMBOLS

Symbol	Definition
$\vec{E}(\vec{r},t)$	Electric field vector.
f	Grating fill factor.
$\vec{H}(\vec{r},t)$	Magnetic field vector.
k_0	Wave propagation constant in vaccum.
$\vec{k}_{inc}$	The incident k-vector.
$\vec{k}_{final}$	The diffracted k-vector.
$\vec{K}_G$	Grating vector.
n	Refractive index.
n_{eff}	Effective refractive index of the propagating mode.
n_{ave}	Volume average of refractive index between the two materials forming the grating.
P_i	Power in the incident fiber mode.
P_{LCE}	Power at detector for light coupled into left side of waveguide.
P_R	Power at the detector for reflection.
P_{RCE}	Power at detector for light coupled into right side of waveguide.
P_T	Power at the detector for transmission.
TE	Only E_z, H_x, and H_y are involved for TE polarization.
TM	Only H_z, E_x, and E_y are involved for TM polarization.

η_{RCE}	Right coupling efficiency to the slab waveguide.
η_{LCE}	Left coupling efficiency to the slab waveguide.
η_R	Optical efficiency of reflection.
η_T	Optical efficiency of transmission.
Δ	Refractive index contrast
Δt	Discrete time step in finite difference time domain.
Δx	Yell cell size along x-direction.
Δy	Yee cell size along y-direction.
θ_s	Grating slant angle relative to waveguide normal.
γ	Complex propagation constants of leaky mode.
α	Radiation factor of leaky mode.
β	The real part of the propagation constant.
λ_o	Wavelength of light in a vacuum.
π	Physical constant pi.
σ	Electric conductivity
ε	Electric permittivity.
μ	Magnetic permeability.
ρ'	Magnetic conductivity
Λ	Grating period.

LIST OF ACRONYMS

Acronym	Definition
2-D FDTD	Two dimensional finite difference time domain
μGA	Micro genetic algorithm
ESGC	Embedded slanted grating coupler
GA	Genetic algorithm
I/O	Input/Output
MOI	Mode overlap integral
OAE	Oxygen atomic etching
PLC	Planar lightwave circuit
PML	Perfectly Matched Layer
RCWA	Rigorous coupled wave analysis
RIE	Reactive ion etcher
SEM	Scanning electron microscope
SLGC	Slanted grating coupler
SMF	Single mode fiber
SWGC	Stratified waveguide grating coupler
SOA	Semiconductor optical amplifiers
SOI	Silicon on insulator

Chapter 1

INTRODUCTION

1.1 Motivation

Since their inception in the 1960s, integrated optical systems have played an important role in advancing and modernizing the telecommunications industry. Within the last decade the free market has invested enormous sums of money into high technology companies specializing in technologies that employ the advances in integrated optical systems. Today, the market continues to grow in a broad spectrum of areas. For example, very small scale, high speed, efficient, on-chip integrated photonic components—switches, transmitters, receivers, and amplifiers—are in demand. As an added advantage, the manufacturing of small scale, integrated components can be efficiently automated with great time savings and cost reduction. Planar lightwave circuits (PLCs), which use existing semiconductor manufacturing processing, offer all these advantages and more. On-chip distributed processor interconnections, more efficient/enhanced information processing and transmission at a considerable cost reduction over electronic on-chip components make PLC a highly desirable technology to pursue. Currently, PLCs based on photonic crystals and high index contrast waveguides are being actively investigated [1] [2] [3] [4]. The desire to migrate to high index

contrast devices is driven by one critical factor: the high optical confinement of high index contrast devices waveguides allows for tighter bend radii and thus reduced die size.

Competition in today's telecommunications market in delivering low cost, highly reliable, and high quality telephone, internet, and video service to the office and home is a driving factor in photonic component and PLCs development. A critical issue associated with their development and implementation is packaging. By far, the most critical aspect of packaging is a precise fiber optic alignment in which PLCs are interfaced with other optical components and devices either by single mode optical fibers or fiber arrays. The difficulty, and challenge, lies in the fact that there is a considerable size differential between the single mode fibers and their interface components, photonic crystals and high index contrast waveguides, which results in a poor mode overlap between them.

At present, alignment and packaging account for greater than 80% of the cost of manufacturing of photonic components. This percentage is far too high to produce a cost effective device. It is apparent that implementation of PLCs in optical systems is dependent on more effective designs and methods related to alignment and packaging, which translate into a manufacturing cost reduction. The thrust of the present dissertation is targeted at this goal; a high efficiency coupling method with fibers oriented normal to the waveguide surface without any intermediate optics, based on strong grating coupling, is proposed and developed. This method has the potential to surmount the difficulties typically associated with coupling between the single mode fibers and high index contrast waveguides for dense PLCs.

1.2 Overview of the dissertation

The focus of this dissertation is the design of high efficiency, compact grating couplers for coupling light between an optical fiber at normal incidence to high index contrast planar waveguides without the use of any intermediate optics. We begin in Chapter 2 by reviewing necessary background information. It begins by reviewing a standing challenge in integrated optics: high efficiency coupling between high index contrast waveguide and single mode optical fiber. It then proceeds with a review of the most widely researched and exploited methods, and points out their limitations which prohibit their use in highly integrated PLCs. This is followed by a discussion of the merits of a grating coupler as an alternative coupling method designed for vertical fiber coupling, and contrasted with more traditional weak grating couplers. The chapter ends with a review of the associated research and a brief description of the numerical tools used.

A novel approach, stratified waveguide grating couplers (SWGC), as a candidate technology, is proposed in Chapter 3. In this approach, the stratified grating couplers consist of three binary grating layers embedded in the upper waveguide cladding with the bottom layer situated on top of the waveguide core. The three layers are shifted relative to each other to create a structure similar to a volume grating with slanted fringes. The light from a fiber positioned vertically to the waveguide surface is incident onto the stratified grating couplers and eventually coupled into the waveguide traveling in one direction. With the design and optimized function of micro-genetic-algorithm two-dimensional finite difference time domain code (μGA 2-D FDTD), simulation results show that ~72% coupling efficiency is possible for fiber (core size 8.3μm and Δ=0.36%

based on Corning SMF-28 single mode optical fiber) to a planar waveguide (1.2μm core and Δ=3.1%) coupling. Further FDTD simulation shows SWGCs have a broad spectrum response and relaxed fiber alignment tolerance. Using a rigorous coupled wave analysis (RCWA) mode solver and K-vector diagram analysis, we found that the phase-matching and Bragg conditions are simultaneously satisfied through the fundamental leaky mode. The tolerance simulation results presented at the end of the chapter show reasonable tolerance, but careful management of the fabrication tolerance is anticipated to be necessary for high efficiency.

Motivated by the development of a slanted etch process at Los Alamos National Laboratory, a second approach called slanted grating coupler (SLGC) with a parallelogramic-shaped profile, is investigated in Chapter 4. The three binary grating layers in the stratified grating coupler are replaced by the single slanted grating layer to avoid the complex alignment procedure required in stratified gratings. Based on the same waveguide materials and the same optical fiber as in Chapter 3, input coupling efficiencies of 66.8% and 80.1% for uniform and non-uniform SLGC, respectively, are achieved with grating optimization by μGA 2-D FDTD. By reciprocal relationship between input coupler and output coupler, calculating the output field gives us more insight into the physics of input couplers, particularly non-uniform input coupler, when the optimized input couplers are used as output couplers. Furthermore, similar conclusions are found with SLGC: phase match conditions and Bragg conditions are satisfied simultaneously, there is a broad spectral response, and a more relaxed fiber alignment sensitivity. Tolerance analysis is evaluated for the optimized uniform SLGC.

The slant angle tolerance (±4º for efficiency drop from 66.8% to 60%) is more relaxed than for a weak grating coupler.

Chapter 5 presents a modified slanted grating coupler, called embedded slanted grating coupler (ESGC). This is especially suitable for waveguides with submicron core size like silicon-on-insulator (SOI) waveguides. Besides the phase matching and Bragg conditions affecting coupling efficiency, fiber mode size proved to have an affect on the coupling efficiency using a reciprocal relationship between the input coupler and the output coupler. μGA 2-D FDTD designs show that up to 69.8% and 75.8% for uniform and non-uniform ESGC, respectively, is possible for a 240nm thick SOI planar waveguide for an optical fiber with core size of 4.4 μm and core and cladding indices of 1.484 and 1.46. It is found that the phase match condition is satisfied but the Bragg condition is slightly off since μGA always try to find a best result that could balance all the factors (phase matching, Bragg condition, and fiber mode matching) affecting the coupling efficiency if the fiber mode cannot be matched well. Similar to SWGCs and SLGCs, ESGCs have a broad spectral response and a more relaxed fiber alignment sensitivity. These turn out to be common features of strong grating couplers. The tolerance simulation results presented at the end of the chapter show a careful management of fabrication tolerance is necessary for high efficiency. Additionally, we apply ESGC to waveguides with the same polymer waveguide materials used in Chapter 3 and 4. Higher coupling efficiency of 85.4% is found because of the smoother mode transition at the grating boundary.

The utility of the μGA 2-D FDTD design and optimization function has proven to be extraordinary as demonstrated in Chapters 3, 4 and 5. However, it is a time

consuming process and requires huge computational resources. Therefore, based on our analysis of strong grating couplers in the previous chapters, a systematic design procedure for uniform slanted grating couplers is developed in Chapter 6 without the aid of μGA optimization. Using this procedure, a specific design example for SOI waveguides proves to be effective. Moreover, the example design confirms the accuracy of our analysis of strong grating couplers using a k-vector diagram with an RCWA mode solver.

A summary of the dissertation research accomplishments is given in Chapter 7, along with a list of suggested future research recommendations.

1.3 New contributions

The salient features of this dissertation research are

1. Strong waveguide grating coupler structures are proposed for vertical fiber coupling to tackle the challenging coupling problem in integrated optics.
2. A new stratified waveguide grating coupler (SWGC) is proposed and investigated for waveguide coupling applications.
3. Slanted grating coupler structures are designed for both polymer waveguide and SOI waveguides.
4. The phenomena associated with strong grating coupling are explained by use of an RCWA mode solver and a simplified K-vector diagram.

5. A systematic design procedure is developed for uniform slanted grating couplers without the design aid of μGA FDTD which is a time consuming process.

Chapter 2

BACKGROUND

Waveguide/fiber interconnection is a critical feature in the use of optical waveguide devices. The large dimensional mismatch between common optical single mode fibers and high index contrast waveguides, and their respective mode sizes, complicates coupling of light from one to the other. In this chapter, a detailed review of the traditional pigtailing method is given. In addition, an overview of several other approaches, found in the literature, including their advantages and disadvantages are given. Finally, the computational tools used in this work are briefly introduced.

2.1 Coupling between high index contrast waveguides and single mode fiber

Planar lightwave circuits (PLCs) typically require waveguides that support only a single fundamental waveguide mode for each of two possible orthogonal polarizations. The cross-sectional dimensions of such single mode waveguides are determined primarily by the free-space wavelength of the guided light, the effective index of the waveguide core, and the refractive index contrast, Δ, between the core and the cladding ($\Delta=(n_{co}-n_{cl})/n_{co}$, with n_{co} and n_{cl} the core and clad refractive indices, respectively). By using a waveguide with a large index contrast one may greatly reduce the core size. For example, polymer waveguides can have a refractive index contrast of 3% or greater, while silicon-

on-insulator (SOI) or polysilicon waveguides with SiO_2 cladding can have a refractive index contrast of over 50%. The dimensions of the corresponding single mode waveguides range from ~1.9μm (polymer) to less than 200nm (SOI). Photonic crystal waveguides have core size ranges similar to those of SOI waveguides and other high index materials. The high index contrast also offers stronger light confinement in the small dimensions, therefore enabling bends to be much smaller.

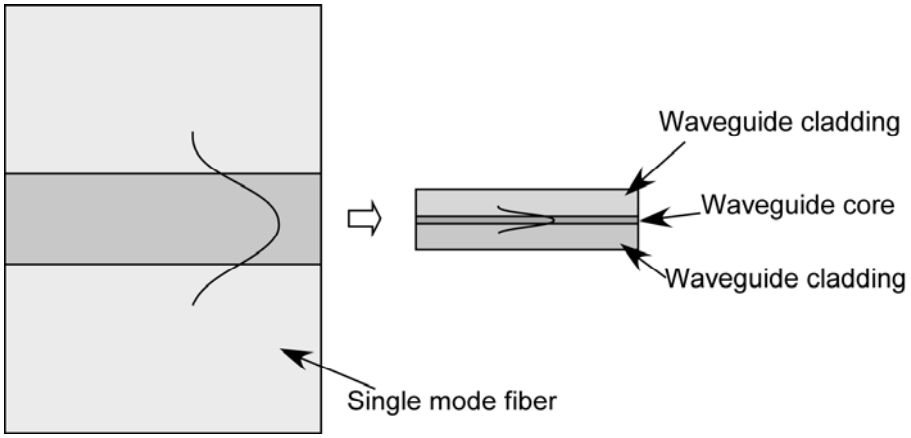

Figure 2.1. Pigtail coupling.

Single mode fibers, however, have a refractive index contrast of <1% and core size typical ~4-9μm. Because of the size mismatch and large numerical aperture (NA) difference, efficient coupling of light between fibers and high index contrast waveguides cannot be accomplished through the traditional method of pigtail coupling in which the end of a fiber is aligned and placed next to the end face of a waveguide. Moreover, alignment is extremely difficult for a waveguide core size of less than 1μm. Obtaining efficient coupling from fiber to high index contrast waveguides has been difficult. Coupling between the fiber and high index contrast waveguides has been a standing

challenge in the field of integrated optics. Alternate coupling methods are therefore required.

2.2 Most widely researched and used methods

The advantages and disadvantages of the most widely used methods are discussed briefly below.

In end-fire coupling, a lens or micro-lens can be used to focus light from a fiber into a high index contrast waveguide. End-fire coupling is often used in the laboratory because of its convenience. However, the alignment tolerance is tight and physical robustness is also an issue. Moreover, the diffraction-limited spot size is often too large to permit efficient coupling into micron and sub-micron waveguide cores.

Another method uses lensed fibers. In this method fibers with a tapered section that terminates in a spherical end achieve a greater numerical aperture than a cleaved and polished fiber end and can therefore be used to couple light with greater efficiency into small-core waveguides. This approach is useful for experimental measurements in the laboratory. It does not, however, offer robust and reliable coupling to sub-micron waveguide cores.

A common approach reported in the literature is the use of tapered couplers [5] [6] [7] [8]. In traditional adiabatic waveguide tapers, the small size waveguide is gradually tapered to a size comparable to the incident fiber core to improve the coupling between the small waveguide and the fiber. In order to avoid radiation loss, the tapering section can be quite long —on the order of one millimeter or more. On the other hand,

inversely tapered waveguides—with a core size of a few hundred nanometers tapered to a small tip of tens of nanometers—can shorten the tapering length to the order of tens of micrometers [8].

An alternative taper technique is to fabricate a second waveguide layer on top of the small size high index contrast waveguide [7]. The top waveguide has a low index contrast and is designed to be single mode with a large core size comparable to the fiber core size. Efficient light coupling first takes place between the incident fiber and this auxiliary waveguide. Then, the light is routed from one layer to the other by means of horizontal and/or vertical tapers of the waveguides in both layers. Tapered couplers are used in commercially available products such as semiconductor lasers and semiconductor optical amplifiers (SOA).

The tapered couplers just introduced share a number of challenges. These include (1) difficulty in achieving vertical tapering; (2) generally complicated processes to fabricate and integrate the tapered structure with other devices; and (3) input/output coupling, I/O, can take place only on the edge of a PLC chip, which limits the number of optical I/Os.

In these three types of methods, input and output coupling take place only on the edge of a chip at the plane of the waveguide device layer. This edge coupling arrangement severely limits the number of optical I/Os in dense PLCs. Moreover, fiber alignment has to be done after the wafer is diced into separate chips, and the end facet of the waveguide needs to be cleaved and polished, which presents taking advantage of the economies of scale long used by the semiconductor industry. As a result, alignment and packaging accounts for the main cost of the manufacturing of optical components.

Indeed, this is a major inhibitor to technological advancements in the telecommunications industry. In order to fully realize the potential of highly integrated PLCs, a new coupling approach scheme needs to be developed, especially one that permits input and output to a 2-D array of fibers.

2.3 Vertical fiber coupling and grating coupler

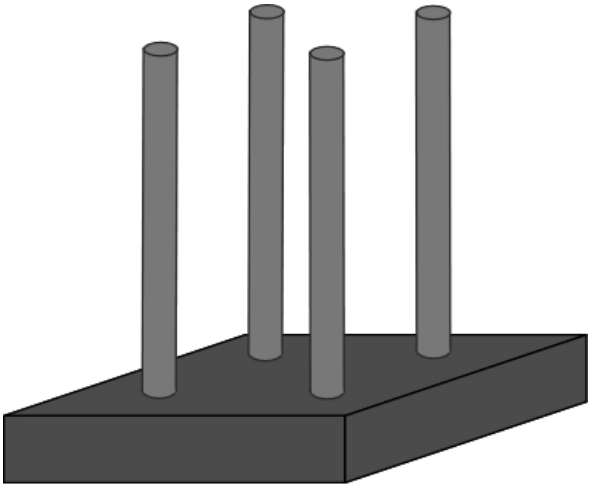

Figure 2.2. Sketch of vertical fiber coupling arrangement.

An alternative to the previously cited approaches is a grating coupler. Grating couplers offer the ability to couple light from out of the plane of the waveguide into (and out of) a waveguide, thereby permitting optical I/Os to populate literally any area of a PLC rather than being confined to just the edge of a PLC chip. This is a very attractive feature, particularly if the incident and exiting light is at normal incidence to the waveguide layer, i.e., fibers are positioned perpendicularly to the surface of waveguides as shown in Figure 2.2.

The vertical fiber coupling approach allows for denser integration because a 2-D array of fibers can be deployed. Furthermore, fiber alignment and PLC testing can be done on the wafer scale and before dicing. Also there is no need to cleave and polish the waveguide ends. Thus, this arrangement results in the possibilities of economies of scale, low manufacturing cost, device density, and miniaturization.

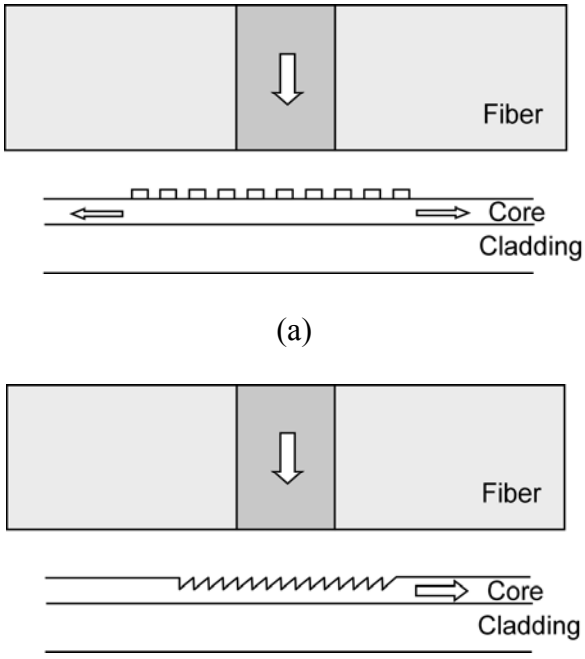

Figure 2.3. Vertical fiber coupling arrangement with (a) symmetric binary grating. (b) asymmetric grating.

Figure 2.3 shows a schematic diagram of the grating coupler geometry we consider to direct light from a fiber at normal incidence to a high index contrast waveguide. The fiber is located in close proximity to the grating without any intermediate optics. The +1 order is excited into the waveguide toward the right. For a symmetric grating coupler such as a binary grating coupler, normal incidence

illumination results in beams propagating in both directions in the waveguide in that the -1 order is excited toward the left as shown in Figure 2.3(b). In order to permit coupling in which wave propagation is in a single direction as shown in Figure 2.3(b), an asymmetric grating structure is required.

In fact, grating couplers are not a new concept. Since being first proposed in the 1970s, grating couplers have been extensively explored both theoretically and experimentally [9] [10] [11] [12] [13] [14] [15] [16] [17] [18] [19] [20] [21] [22] [23] [24]. This work, however, has focused on the weak coupling regime, in which the grating is shallow or the grating refractive index is nearly the same as the cladding or core. This assures that the effect of grating on the waveguide is small and can be treated as a perturbation. In order to get high efficiency, the grating length has to be rather long—at least several hundred μms. To reach maximum efficiency, it is necessary that the incident beam is around the grating length. The maximum coupling efficiency for both Gaussian beams and plane waves is approximately 80% in theory for a uniform grating. In order to get a higher efficiency, larger than 90%, a variable grating depth can be exploited. For the traditional grating coupler with weak coupling and normal incidence, however, the coupling efficiency for fiber/waveguide interconnection is so poor that it appears a grating coupler cannot be used with PLCs. The main reason is because the lateral beam size of a standard single mode fiber is only on the order of tens of microns.

In addition to poor coupling efficiency, the highly dispersive properties of gratings and fabrication difficulties have prevented grating coupler technology from being implemented into PLCs [25].

A high optical coupling efficiency is very desirable for grating couplers to become truly practical, especially for fiber perpendicular to the surface into waveguides without any intermediate optics. In order to get high efficiency over 10's of microns grating length, the grating has to operate in the strong coupling regime. The concept of our strong grating couplers will be introduced in a later chapter.

2.4 Research review for vertical fiber coupling

Until now, there has not been much research reported on grating couplers that work in vertical fiber coupling to waveguide. Besides the present work there is only one reference that we are aware. Taillaert et al. [26] at Ghent University in Belgium proposed independently the same fiber arrangement as us. That is, the incident fiber is oriented normally to the waveguide substrate and located in close proximity to the grating such that no intermediate optics is required. Figure 2.4 shows the structure they designed.

Even though their solution parallels ours, their design is nevertheless quite different. The coupling grating with binary shape is etched deeply into the core. A maximum efficiency of 20% is obtained as calculated with the eigenmode expansion technique for the structure with only coupling grating. Since a symmetric grating and normal incidence are used, light is coupled to the left at the same time as it is to the right. In order to avoid left-coupled light, a reflecting grating is put next to the coupling grating. The maximum efficiency is now 38%. To improve the efficiency further and reduce the transmitted light, a multilayer reflector is put under the waveguide. The maximum simulation result was 74%.

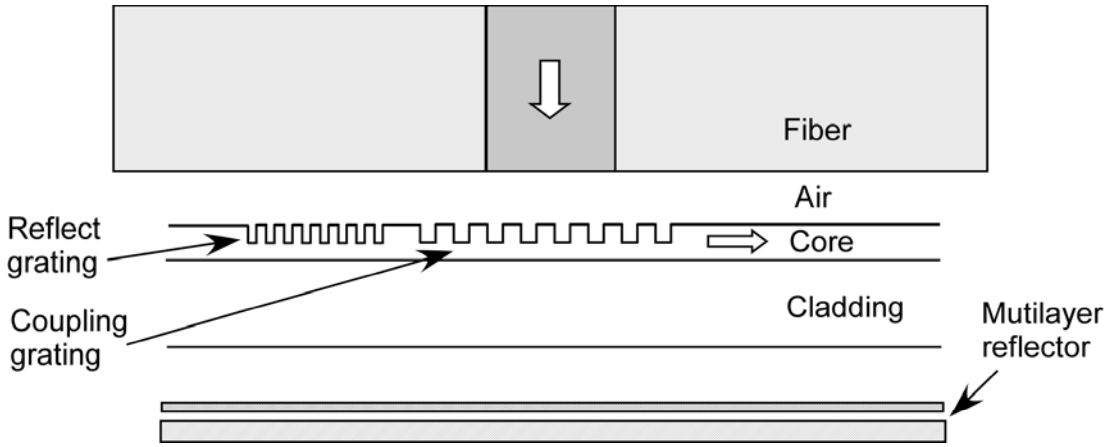

Figure 2.4. Vertical fiber coupling arrangement proposed by Taillaert et al. (IEEE Journal of Quantum Electronics, Vol.38, No.7, July 2002).

2.5 Computational tools

The present work employed 2-D FDTD, μGA-FDTD, RCWA mode solver methods. The RCWA was also used calculate reflectance. Brief information about these methods is given here. A more detailed account of these methods may be found in the references cited.

2.5.1 Two-dimensional finite difference time domain (2-D FDTD) method

Unlike in the more conventional approaches where gratings operate in the weak coupling regime and can be treated as a perturbation on the action of the waveguide, our couplers operate in the strong couple regime and require a non-perturbative analysis.

On the other hand, rigorous electromagnetic grating theories such as rigorous coupled wave analysis (RCWA) [27] cannot be applied because of the finite extent of the

grating coupler. Taillaert et al. [26] employed an eigenmode expansion method in the simulation of their device. Unfortunately, this method will be inefficient in computation if applied to our case of slanted shape of the grating. Owing to the need to divide each grating unit cell into a number of rectangular sub-cells to approximate the slant of the grating, we have therefore applied the finite difference time domain (FDTD) method [28] to rigorously analyze and simulate the strong grating couplers.

The starting point for the FDTD formulations is the two Maxwell curl equations. They can be recast into the following form:

$$\frac{\partial \vec{H}(\vec{r},t)}{\partial t} = -\frac{1}{\mu}\nabla \times \vec{E}(\vec{r},t) - \frac{\rho'}{\mu}\vec{H}(\vec{r},t)$$

$$\frac{\partial \vec{E}(\vec{r},t)}{\partial t} = \frac{1}{\varepsilon}\nabla \times \vec{H}(\vec{r},t) - \frac{\sigma}{\varepsilon}\vec{E}(\vec{r},t) \ , \qquad (2.1)$$

where σ is the electric conductivity for lossy dielectric material and ρ' is magnetic conductivity for magnetic loss. For simplicity we consider the material to be lossless, e.g., $\sigma = 0$ and $\rho' = 0$. We further write out the vector components of the curl operators in equations to yield the following six system components:

$$\frac{\partial H_x}{\partial t} = \frac{1}{\mu}\cdot\left(\frac{\partial E_y}{\partial z} - \frac{\partial E_z}{\partial y}\right), \qquad (2.2)$$

$$\frac{\partial H_y}{\partial t} = \frac{1}{\mu}\cdot\left(\frac{\partial E_z}{\partial x} - \frac{\partial E_x}{\partial z}\right), \qquad (2.3)$$

$$\frac{\partial H_z}{\partial t} = \frac{1}{\mu}\cdot\left(\frac{\partial E_x}{\partial y} - \frac{\partial E_y}{\partial x}\right), \qquad (2.4)$$

$$\frac{\partial E_x}{\partial t} = \frac{1}{\varepsilon}\cdot\left(\frac{\partial H_z}{\partial y} - \frac{\partial H_y}{\partial z}\right), \qquad (2.5)$$

$$\frac{\partial E_y}{\partial t} = \frac{1}{\varepsilon} \cdot (\frac{\partial H_x}{\partial z} - \frac{\partial H_z}{\partial x}), \tag{2.6}$$

$$\frac{\partial E_z}{\partial t} = \frac{1}{\varepsilon} \cdot (\frac{\partial H_y}{\partial x} - \frac{\partial H_x}{\partial y}). \tag{2.7}$$

Generally, in FDTD code, these equations are expressed in linearized form by means of central finite differencing the electromagnetic field components located on a Yee cell. Only nearest-neighbour interactions need be considered as the fields are advanced temporally in discrete time step Δt over spatial cells of rectangular shape $\Delta x \times \Delta y$.

In this dissertation, the 2-D finite difference equations for the TE polarized case are presented. For the TE polarization, only E_z, H_x, and H_y are involved and are governed by the time-dependent Maxwell's equations as the following equations. The electric field component is pointed out of the horizontal plane and two magnetic field components are within the horizontal plane.

$$\frac{\partial H_x}{\partial t} = \frac{1}{\mu} \cdot (-\frac{\partial E_z}{\partial y}), \tag{2.8}$$

$$\frac{\partial H_y}{\partial t} = \frac{1}{\mu} \cdot \frac{\partial E_z}{\partial x}, \tag{2.9}$$

$$\frac{\partial E_z}{\partial t} = \frac{1}{\varepsilon} \cdot (\frac{\partial H_y}{\partial x} - \frac{\partial H_x}{\partial y}). \tag{2.10}$$

The 2-D Yee cell grid is shown in Figure 2.5 for illustration. The magnetic field components at time $(n+1/2)\Delta t$ are located on the sides of the Yee cell while the electric field components at times $n\Delta t$ are located at the center of the Yee cell (n is integer).

Taking account that the grid discretizations in the x- and y- directions are not uniformly equal, the central finite-difference expressions for the TE case are given by

$$H_x\,|_{i,j}^{n+1/2} = H_x\,|_{i,j}^{n-1/2} - \frac{\Delta t}{\mu_{i,j}\Delta y}[(E_z\,|_{i,j+1/2}^{n} - E_z\,|_{i,j-1/2}^{n}), \tag{2.11}$$

$$H_y\,|_{i,j}^{n+1/2} = H_y\,|_{i,j}^{n-1/2} + \frac{\Delta t}{\mu_{i,j}\Delta x}[(E_x\,|_{i+1/2,j}^{n} - E_x\,|_{i-1/2,j}^{n}), \tag{2.12}$$

$$E_z\,|_{i,j}^{n+1} = E_z\,|_{i,j}^{n} + \frac{\Delta t}{\varepsilon_{i,j}}[(H_y\,|_{i+1/2,j}^{n+1/2} - H_y\,|_{i-1/2,j}^{n+1/2})/\Delta y$$

$$-(H_x\,|_{i,j+1/2}^{n+1/2} - H_x\,|_{i,j-1/2}^{n+1/2})/\Delta x]. \tag{2.13}$$

Here we denote a space point in the uniform rectangular grid as $(i, j) = (i\Delta x + j\Delta y)$. Δx and Δy are the grid space increment in the x and y coordinate directions, i and j are integers. Any field u of space and time calculated at a discrete point in the grid and at a discrete point in time is denoted by $u(i\Delta x, i\Delta y, n\Delta t) = u_{i,j}^{n}$, where Δt is the time increment and n is integers.

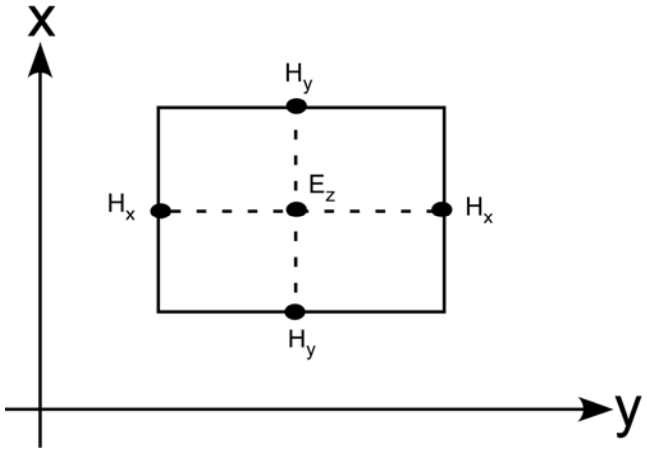

Figure 2.5. Position of the electric and magnetic field vector components about 2-D unit cell of the Yee space lattice for TE polarization calculation.

All component H_x and H_y computations in the FDTD grid space are completed and stored in the computer memory for a particular $(n+1/2)\Delta t$ of time point using the E_z data at $n\Delta t$ time previously stored in the computer memory. Then all of the E_z calculation at $(n+1)\Delta t$ time is completed in the FDTD grid area and stored in the computer memory using the component H data previously computed. This process continues until the time-marching is finished.

2-D FDTD codes have been developed by Dr. Jianhua Jiang and Dr. Jingbo Cai of the Nano and Mirco Devices Center (NMDC) at the University of Alabama in Huntsville [29] [30]. The Berenger Perfectly Matched Layer (PML) boundary condition [31] is employed in both 2-D FDTD codes which can match the impedance of free space and absorbs electromagnetic energy incident at any angle for any frequency.

2.5.2 Micro genetic algorithm (μGA) with 2-D FDTD

To quickly and efficiently explore structural parameters and optimize them, we apply a parallel rigorous design tool recently developed by our group. This design tool employs a parallel small population size genetic algorithm, called micro-GA (μGA) [32] as the global optimization method and a 2-D FDTD method for rigorous electromagnetic computation. GAs [33] are patterned after natural evolutionary processes, e.g., survival of the fittest. Because their robustness and efficiency, GAs haven been intensively used in many field including photonics design. Compared to conventional GA (CGA), our μGA is more computationally efficient because of its small population size with 5 individuals [34]. Like the conventional GA, μGA involves the same procedure, which includes chromosomal coding of the problem parameters, evaluation of the fitness function,

selection methods for survival of the fittest individual, and breeding of new individuals for the next iteration of this process which is called a generation. It is straightforward to apply μGA to a design by simply encoding the structural parameters as float variables in μGA. Dependent variables which can be varied as a function of one or more independent variables are also available in our code. We found that dependent variables provide much more flexibility for complicated geometry control, which is often required in the design of complex photonic design. However, it is critical to define a proper fitness (or objective) function for the success of the μGA optimization. The fitness function of a structural optimization is defined as

$$f = c(1-\eta), \tag{2.14}$$

where c is a positive scaling coefficient. The purpose of μGA optimization is to minimize f and therefore maximize η which is coupling efficiency here. In grating coupler case, η is the coupling efficiency. Usually it takes approximately at least 100 μGA generations to converge to an optimal grating coupler design. The combination of μGA and 2-D FDTD is unique and powerful, and has been successfully to design some diffractive optical elements, photonic devices like air trench waveguide bend and beam splitters [35][36][37].

2.5.3 Rigorous Coupled-Wave Analysis (RCWA) mode solver and reflectance calculation for grating structures with any profile

While our rigorous numerical design tool, μGA-2D FDTD, is well suited for the design of strong grating couplers, it does not give us intuitive insight into the principles of strong grating coupler operation due to the built-in random process of μGA and the

pure numerical nature of FDTD. To physically analyze the μGA optimized strong grating coupler designs, it is crucial to find the leaky mode characteristics of the strong grating coupler, i.e., waves guided by the grating structures. This is complicated by the fact that the presence of the grating strongly affects the waveguide mode, which is not the case for gratings that operate in the weak coupling regime.

We therefore use a rigorous grating theory, the Rigorous Coupled-Wave Analysis (RCWA) method, to solve the so-called homogeneous problem [38] for strong grating couplers for the complex propagation constants $\gamma_m = \beta_m + i\alpha_m$ (m is the mode index) of the leaky modes supported by the grating coupler structures. The real part of the propagation constant, β_m, is responsible for the phase-matching condition of strong grating coupler as will be discussed later and α_m is the radiation factor of the leaky modes, which determines the optimized coupling length of the grating coupler. We will skip the detail and tedious mathematical formulations of the RCWA procedure and refer the interested reader to the literature, such as Ref. [39] for example, for the details. Also, the well-known Muller root searching algorithm [40] is used to find the zeros of the determinant of the RCWA characteristic matrix. To apply RCWA, the proposed finite length strong grating couplers have to be infinitely extended in the x direction.

Abnormal reflectance may be found when the excitement of the fundamental leaky mode and Bragg diffraction present in a grating coupler structure. To calculate the reflectance scattered by a dielectric grating having an arbitrary periodic profile, the mathematical procedure is similar to the above mode calculation with the one exception that the incident wave must be a plane wave.

Chapter 3

STRATIFIED WAVEGUIDE GRATING COUPLER FOR NORMAL FIBER INCIDENCE

Previous work in the Nano and Micro Devices Center at UAH on stratified gratings for non-waveguide applications [41] [42], demonstrated that microfabricated stratified gratings can yield high diffraction efficiency similar to volume gratings. In this chapter, I investigate their use as high efficiency waveguide couplers. A stratified waveguide grating coupler for coupling light from a fiber at normal incidence into a planar waveguide is proposed. SWGCs are designed to operate in the strong coupling regime without intermediate optics between the fiber and waveguide. Two-dimensional finite difference time domain simulation in conjunction with micro genetic algorithm optimization shows that ~72% coupling efficiency is possible for fiber (core size 8.3μm and Δ=0.36%) to slab waveguide (1.2μm core and Δ=3.1%) coupling. A rigorous mode analysis reveals that phase-matching and Bragg conditions are satisfied simultaneously with respect to the fundamental leaky mode supported by the optimized SWGC. The work in this chapter has been published in Optics Letters (Vol.30, No.8, 2005) [43].

3.1 Strong grating coupler for vertical fiber coupling

I will now briefly discuss the salient features of our design concepts for strong grating couplers with a vertical fiber coupling before proceeding with the specific details related to the design structure of stratified grating couplers in this chapter and grating couplers with a slanted profile in Chapter 4 and Chapter 5. These features form the fundamental material on which the present dissertation is built.

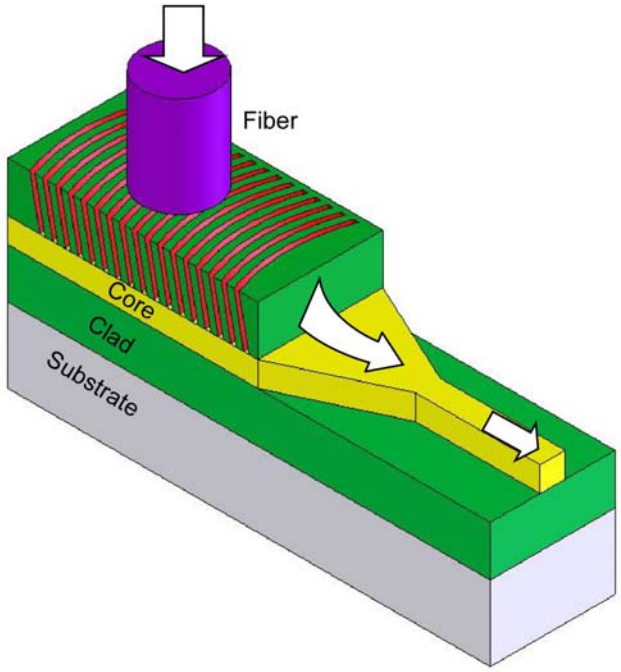

Figure 3.1. 3D geometry of the strong grating coupler for normal coupling between fiber and waveguide.

Figure 3.1 shows the 3D geometry of our strong grating coupler. As seen in Figure 3.1, the strong grating coupler utilizes a grating to couple light from a normally oriented fiber into a waveguide without any intermediate optics. There are two essential

criteria for this coupling scheme to be functional. Firstly, the incident light must traverse an angular path of 90^0 from the fiber to waveguide. Secondly, the broad grating ridge needs a semicircular geometry in order to first focus the light into the lateral waveguide which is laterally tapered, and then into the single mode channel waveguide.

In order to get high efficiency over a short (10 to 20 microns) grating length, the grating must operate in the strong coupling regime. There are two main features of our grating coupler design. First, the employment of an asymmetric grating profile is necessary to break the symmetry problem associated with the surface normal coupling between fiber and planar waveguide. A properly designed asymmetric grating structure can therefore unidirectionally couple light into the desired waveguide direction and suppress coupling in the opposite direction. Thus both the first-order grating reflector and the bottom reflector in Taillaert's [26] design (introduced in Chapter 2), can be eliminated. Second, our strong grating couplers utilize strong index modulation gratings to further strengthen the coupling effect and keep the length of the coupler short. The strong index modulation is introduced by means of a high index material for the grating ridges and a grating thickness on the order of a wavelength. All these features enable us to realize efficient and compact grating coupler designs.

In this dissertation, we investigate high efficiency 90º coupling from the fiber to waveguide using a grating coupler and we consider only 2D simulations for TE polarization (electric field is out of the paper plane). It is expected that coupling efficiency in 3D structure will be lower than for the 2D case.

3.2 Design and simulation

The basic 2D geometry of a SWGC is shown in Figure 3.2. In this particular example, the SWGC consists of three binary grating layers embedded in the upper cladding of the waveguide with the bottom-most layer situated on top of the waveguide core. Since the layers in the SWGC are fabricated sequentially, the binary grating layers can be laterally shifted relative to one another to create a stratified grating structure analogous to a volume grating with slanted fringes. This allows an element to be designed with high diffraction efficiency into the first order for any arbitrary angle of incidence. In particular, a grating with maximum first order efficiency at normal incidence can be achieved using this technique. The refractive index difference between the grating material and the cladding can be quite large—0.3 to 2.0—depending on the choice of materials. This high index contrast significantly strengthens the coupling effect, so that shorter grating lengths (10μm -20μm), comparable to the mode field diameter of a fiber, are sufficient for high efficiency coupling.

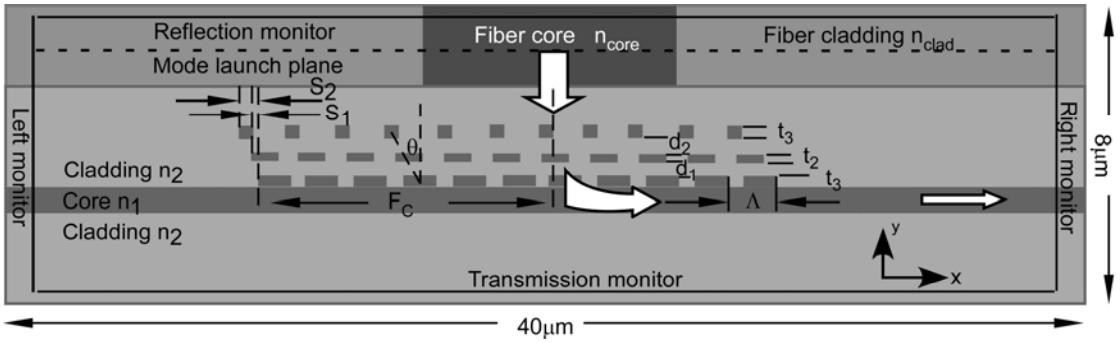

Figure 3.2. SWGC geometry for FDTD simulation.

Since there are no prior restrictions on the thickness of any grating layer and the gratings have only approximately 20 periods, the traditional grating coupling theory, like perturbation theory, is not accurate. This is because the traditional theory treats the grating either as a small perturbation or of infinite extent, neither of which are valid for our strong coupling regime. Since SWGCs operate in the strong coupling regime we have employed a 2D-FDTD method [28] with Berenger's PML boundary conditions [31] to accurately simulate its behavior. As shown in Figure 3.2, the fundamental mode of the fiber waveguide is sourced at the top of the FDTD simulation region, propagates toward the grating coupler, and is eventually coupled into the waveguide traveling to the right. Four FDTD field and power monitors are defined in Figure 3.2 for monitoring the optical efficiency of reflection (η_R) back toward the input space, transmission (η_T) into the lower cladding, and left and right coupling efficiency (η_{LCE} and η_{RCE}, respectively) to the slab waveguide. These parameters are calculated from FDTD simulation results by

$$\eta_{RCE} = \frac{P_{RCE}}{P_i} \times MOI \tag{3.1}$$

$$\eta_j = \frac{P_j}{P_i}, \qquad with\ j = R, T, LCE, \tag{3.2}$$

where P_i is the power in the incident fiber mode, and P_j and P_{RCE} are the total power detected on each monitor. The *MOI* term in Equation 3.1 is the mode overlap integral between the actual FDTD field distribution detected on a monitor and the analytical mode profile of the waveguide at the specific location of the monitor. The *MOI* indicates how much of the power detected on the monitor will actually be guided by the waveguide. Further detail about *MOI* calculation may be found in references [44] [45].

A number of parameters need to be optimized to maximize the coupling efficiency of a SWGC. These include the grating period, Λ; grating thicknesses, t_1, t_2, t_3; fill factors (i.e., grating ridge width divided by grating period), f_1, f_2, f_3; homogeneous layer thicknesses, d_1, d_2; and lateral shift of the middle and top layers relative to the bottom layer, s_1, s_2. The x-coordinate of the center of the fiber, F_c, relative to the left edge of the bottom grating must also be optimized to properly position the incident optical field with respect to the grating. This involves a balance between outcoupling the incident light if the fiber is positioned too far to the left and not intersecting enough of the incident light if the fiber is positioned too far to the right. To rapidly search the large parameter space encompassed by the above variables, we apply the design tool in [29], which employs a parallel μGA as the global optimization method and 2D-FDTD as the rigorous electromagnetic computational core.

As shown in Figure 3.2, we consider a single mode slab waveguide with a core thickness of 1.2μm (n_1=1.5073) embedded in a cladding with n_2=1.4600 (refractive index contrast Δ=3.1%). We assume a grating ridge material of TiO_2 with refractive index, n_g, of 2.300. The fiber is simulated as a 2D slab waveguide with the following parameters: 8.3μm core, n_{core}=1.4700, n_{clad}=1.4647 and Δ=0.36%. The entire structure is simulated using a FDTD region of 40μm×8μm. The Yee cell size [28] is 18nm in both the x and y directions. The central wavelength in free space is λ=1.55μm and only TE polarization (electric field out of the paper plane) is considered here. We assume a grating with 22 periods.

First, simulation results for a single grating layer are shown in Figure 3.3. The magnitude squared of the time-averaged electric field is shown as a gray image

superimposed over an outline of the waveguide, grating and fiber. The scale represents the power per area (irradiance) with the peak of the incidence amplitude normalized to 1. Due to the symmetry of the geometry, the incident light is coupled into both directions of the waveguide. Since the fiber is positioned far to the left side of grating, light coupled into the left is coupled out again. In this case, the coupling efficiency into the right direction is 25 %.

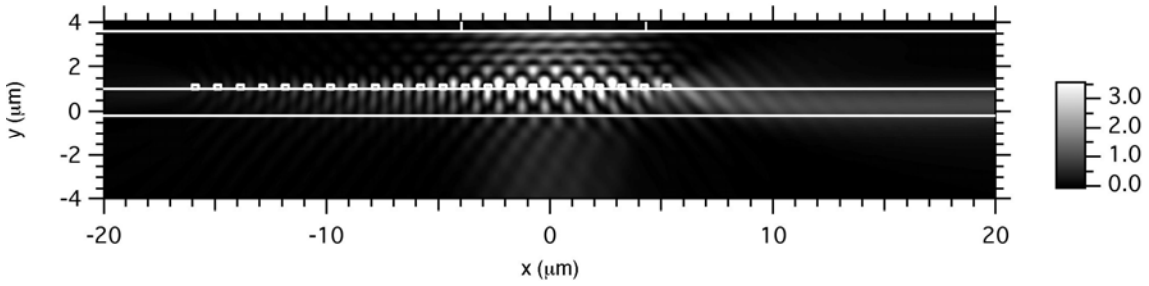

Figure 3.3. The μGA FDTD optimized result of magnitude squared time averaged E_z component with single binary grating layer.

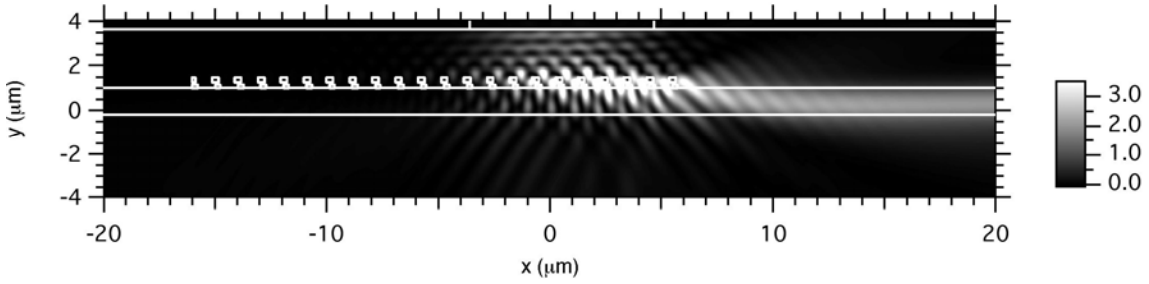

Figure 3.4. The μGA FDTD optimized result of magnitude squared time averaged E_z component with double binary grating layer.

The addition of a second shifted grating layer, shown in Figure 3.4, breaks the symmetry of the coupler and enables a coupling into a single direction for an appropriate choice of grating separation and shift. The coupling efficiency for light propagating to the right is 52%. Most of the light is transmitted through the structure with only a small amount being reflected. This result graphically demonstrates the utility of using multiple gratings to force the coupled light to diffract in only one direction in the waveguide for normally incident illumination.

Table 3.1 Structural parameters for SWGC with three grating layers

Parameter	Value	μGA search Range Min-Max
Grating Period Λ (μm)	1.025	1.0-1.1
Top grating fill factor f_3	0.21	0.1-0.7
Middle grating fill factor f_2	0.36	0.1-0.7
Bottom grating fill factor f_1	0.23	0.1-0.7
Top grating thickness t_3 (μm)	0.817	0.05-1.5
Middle grating thickness t_2 (μm)	0.072	0.05-1.5
Bottom grating thickness t_1 (μm)	0.162	0.05-1.5
Thickness of top homogeneous layer d_2 (μm)	0.207	0.0-0.6
Thickness of middle homogeneous layer d_1 (μm)	0.072	0.0-0.6
Relative x-position of middle layer s_1 (μm)	0.236	0.0-3.0
Relative x-position of top layer s_2 (μm)	0.546	0.0-3.0
X coordinate of center of fiber F_c (μm)	15.27	8.0-18.0

Our previous RCWA simulations for free space application have shown that the diffraction efficiency of a stratified grating structure depends on the number of grating layers [41]. Simulations with three grating layers are also investigated here. The parameters for the final optimized three-layer SWGC's are listed in Table 3.1, along with the range of parameter values searched in the μGA optimization. Figure 3.5 shows the optimized SWGC geometry superimposed on the magnitude squared time averaged electric field. Note the excellent coupling of the field into the mode supported by the waveguide. The corresponding power ratios (i.e., power detected on a given monitor to the power launched) are 76.18% for power directed to the right, 4.62% for power directed to the left, and 12.26% and 6.93% for power transmitted and reflected by the SWGC, respectively. The *MOI* shows that the efficiency with which power is directed from the fiber into the mode supported by the waveguide is 71.6%.

Also note that there is some scattering loss at the boundary between the grating region and the output slab waveguide. Note also that, the centers of the high index regions in the three grating regions are positioned at an angle of θ=33.78° with respect to the surface normal, which is analogous to a slanted fringe in a volume holographic grating.

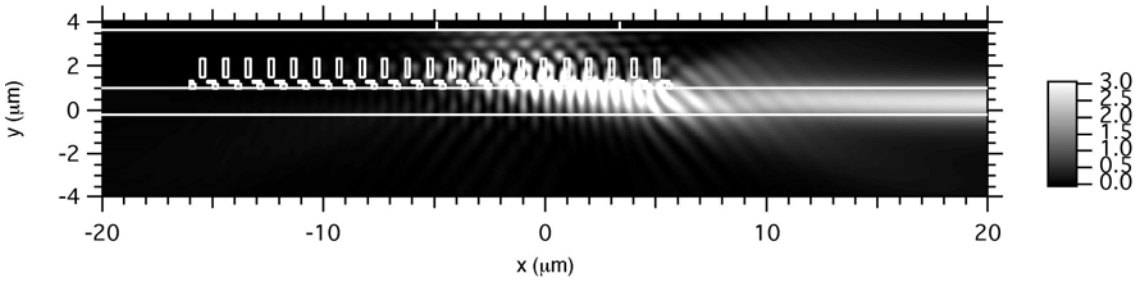

Figure 3.5. Magnitude time averaged electric field calculated with 2-D FDTD.

3.3 Physical analysis and discussion

While our rigorous numerical design tool, μGA-2D FDTD, is well suited for the design of SWGC, it does not, however, give intuitive insight into the principles of SWGC operation. This is due to the built-in random process of μGA, and the purely numerical nature of the FDTD. To physically analyze the μGA optimized SWGC designs, it is crucial to find the leaky mode characteristics of the SWGC. Things are complicated further by the fact that the presence of the grating strongly affects the waveguide mode. This is not the case for gratings that operate in the weak coupling regime.

We will first examine the leaky modes of the SWGC design in Figure 3.5. Because the SWGC is designed as an input coupler for coupling light to the right in the waveguide, only the forward propagating leaky modes with positive β_m are responsible for the coupling and will be the only modes considered. At λ_0=1.55μm the two of the lowest order leaky modes are found for this SWGC: a fundamental mode with $\gamma_0=\beta_0+i\alpha_0$=6.1329+i0.4732 and a higher order mode with $\gamma_1=\beta_1+i\alpha_1$= 5.9780+i0.2243. We can define the effective index of a leaky mode as

$$n_m = \beta_m / k_0 , \tag{3.3}$$

where k_0 is the wave propagation constant in vacuum. With this definition, the effective indices of the fundamental and higher order mode are 1.5128 and 1.4747, respectively. On the other hand, a simple mode analysis of the single mode in a 2D slab waveguide reveals that the effective index for the fundamental mode is 1.4797.

Equipped with accurate mode effective indices, we can now investigate the phase-matching condition of strong coupling SWGC's. In general, the phase matching of the grating can be expressed with the well-known grating equation as [9]

$$\beta_{qx} = k_{ix} + q.2\pi / \Lambda, \qquad q = 0,\pm1,\pm2\cdots, \tag{3.4}$$

in which k_{ix} is the x-component of the incident k vector, Λ is the grating period in the x direction, and q is the diffraction order of the slanted grating. For surface normal incidence k_{ix} is zero. For the μGA optimized value of Λ=1.025μm, it is easy to see that the phase-matching condition of the SWGC can be satisfied with respect to the fundamental leaky mode when q=1. In other words, the +1 diffraction order of the grating provides the required phase matching between the incident fiber mode and the fundamental leaky mode of the SWGC. Note that this phase-matching mechanism is very different from that of conventional weak grating couplers. In weak grating couplers, even though the +1 diffraction order is also responsible for phase matching, the phase matching is always assumed to be realized for the unperturbed waveguide mode, and the period of the coupler can be analytically calculated. However, analytical determination of the grating period of our SWGC from the phase-matching condition is impossible because the fundamental leaky mode of the SWGC's is a function of all of grating parameters, including the grating period itself. Consequently, realization of the phase-matching condition must be part of the SWGC's design process. In this sense, the design and optimization of the SWGC's is far more complicated than weak grating couplers.

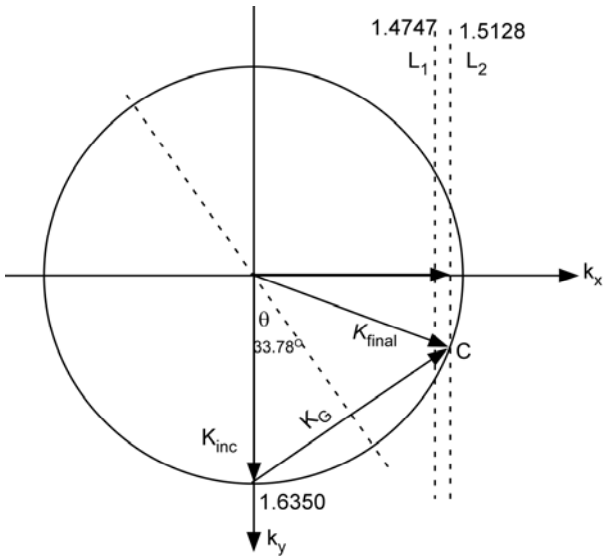

Figure 3.6. K-vector diagram of SWGC.

The phase-matching condition of the SWGC suggests that its fundamental leaky mode plays a central role. A further k-vector diagram analysis of the SWGC is constructed to confirm that the Bragg condition is satisfied.

The k-vector diagram for the SWGC is shown in Figure 3.6. Note that all k vectors in the figure have been normalized by a division with k_0 for convenience and are dimensionless. As a first order approximation, the stratified grating of the SWGC can be treated as a homogeneous layer with an average refractive index, n_{av}, defined as the volume average between the two materials forming the grating ridge shape [46] [47]:

$$n_{av} = \left\{ \left[\sum_{i=3} \left[\left(n_1^2 \times f_i + n_2^2 \times (1 - f_i) \right] \times t_i + \sum_{m=2} n_2^2 \times d_m \right] \Big/ \left[\sum_{i=3} t_i + \sum_{m=2} d_m \right] \right\}^{1/2}, \quad (3.4)$$

in which all of the symbols have the same definitions as in Figure 3.2. The solid circle with a radius of 1.6350 denotes this effective index for the grating layer. $\vec{K}_{inc}$ is the

normally incident k-vector and the dotted slanted line refers to the orientation of the slanted fringe relative to the k_y axis, which is 33.78° in this case. The two dotted vertical lines L_1 and L_2 at k_x = 1.4747 and 1.5128 correspond to the effective indices of the waveguide mode and the fundamental leaky mode, respectively. If we draw the grating vector $\vec{K}_G$ perpendicular to the orientation of the slanted ridges, the diffracted k-vector, $\vec{k}_{final}$, which is equal to vector sum of ($\vec{K}_{inc} + \vec{K}_G$), terminates on L_2 which satisfies the phase matching condition. If the Bragg condition is obeyed, the diffracted k-vector, $\vec{k}_{final}$, will terminate on the circle. As seen in Figure 3.6, this is the case. It is clear from this k-vector diagram that the Bragg diffraction condition is simultaneously satisfied for the +1 diffraction order of the slanted grating while phase matching between the incident fiber mode and the fundamental leaky mode of the SWGC is also satisfied. Bragg diffraction suppresses other diffraction orders and therefore enforces unidirectional coupling of the SWGC. Note that finding a SWGC design that simultaneously satisfies phase matching and the Bragg condition for a grating that operates in the strong coupling regime strongly demonstrates the powerful optimization capability of our μGA-2D FDTD design tool.

Further 2D-FDTD simulation of the three-layer structure shows that the SWGC design has a relatively broad spectral response and a reasonable lateral fiber misalignment tolerance. Over the range wavelengths from 1.52 to1.57μm, there is at most an additional 1.5 dB coupling loss compared to the loss at 1.55μm, and a lateral shift of ±3μm results in less than 1 dB of additional coupling loss. This is shown in Figure 3.7(a) and Figure 3.7(b), respectively. On the plots, the squared points are those simulated by the FDTD.

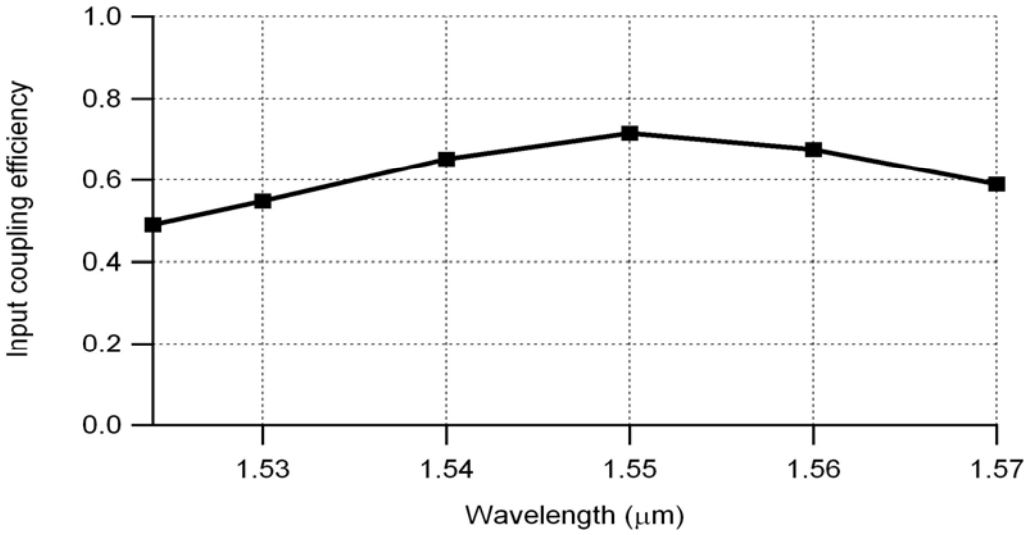

(a)

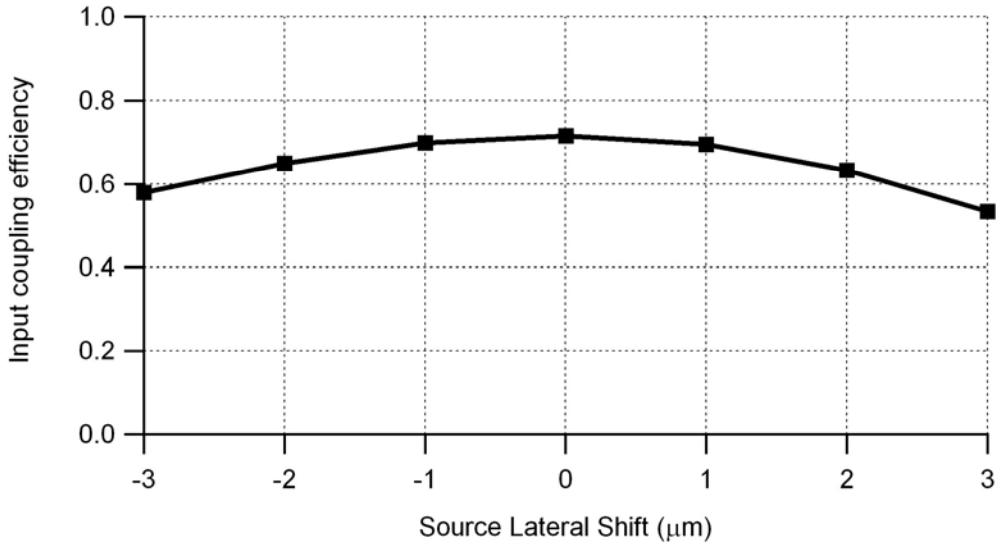

(b)

Figure 3.7. (a) Spectral response of the SWGC. (b) Lateral shift sensitivity analysis of the SWGC based on a fiber lateral shift as in Figure 3.5.

3.4 Fabrication tolerance

We now examine the fabrication tolerances for the layer-to-layer alignment, grating layer thickness, ridge width, and the homogenous layer thickness. The criterion for the tolerance is the efficiency being reduced from the optimized value of 71.6% to 60%. The other parameters keep being optimized while one parameter is tested. The tolerance for relative grating shift is 40nm for the top grating and 70nm for the middle one. The tolerance for the homogenous layer thickness is 70nm and grating thickness is 144nm (17.6%), 25nm (34.7%), and 50nm (31%) for the top, middle, and bottom layers respectively. Likewise, the grating ridge width tolerance is 70nm (32.35%), 180nm (48.8%), and 40nm (17%) for the top, middle, and the bottom layers. We anticipate that careful management of the fabrication tolerance will be necessary for the successful fabrication of high efficiency SWGCs.

Also note that all the above simulation results are limited to TE polarization. Simulation of the same structure, but for a TM polarization results in a very low coupling efficiency—approximately -20dB.

3.5 Conclusions

In this chapter, we have demonstrated that SWGCs offer a potentially viable method to couple TE polarized light from a fiber at normal incidence into a small core waveguide with high efficiency. An important next step in evaluating the properties of SWGCs is to extend the 2-D results to a 3-D analysis of SWGCs.

Chapter 4

COMPACT SLANTED WAVEGUIDE GRATING COUPLER

In this chapter, we propose a slanted grating coupler (SLGC) with a parallelogramic-shaped profile in which high coupling efficiency can be achieved with a single grating layer that operates in the strong coupling regime [48]. We were originally motivated to examine such structures by the development of a new etching technique that readily achieves slanted etches and avoids the complicated alignment procedure in SWGC. The work in this chapter has been published in Optics Express (Vol.12, No.15, pp.3315-3326, 2004) [48].

4.1 Motivation

Slanted grating couplers with a parallelogramic-shaped profile have been examined both theoretically and experimentally by Matsumoto [49], Li [50] [51] [52] and Tishchenko [53] for the weak coupling case to obtain the performance of a volume grating at Bragg angle. Their studies reveal that parallelogramic shaped gratings are excellent for coupler applications because they generally have a larger radiation factor and higher radiation directionality compared to other grating profiles. To achieve the slanted profile, a standard lithographic technique (usually e-beam lithography) is used to make a binary mask in photoresist or metal and then the substrate is tiled at the desired slanted angle in etching process.

Fabrication of the slanted grating coupler for our fiber incidence application is more challenging than for weak coupling applications because the grating with a high aspect ratio needs to be etched on a high index material.

A slanted grating with an aspect ratio of about 5:1 was realized in photoresist (n=1.6) by use of direct electron beam writing and reactive ion etching [54]. The slanted grating along x direction is Λ =0.598μm and f=0.35.

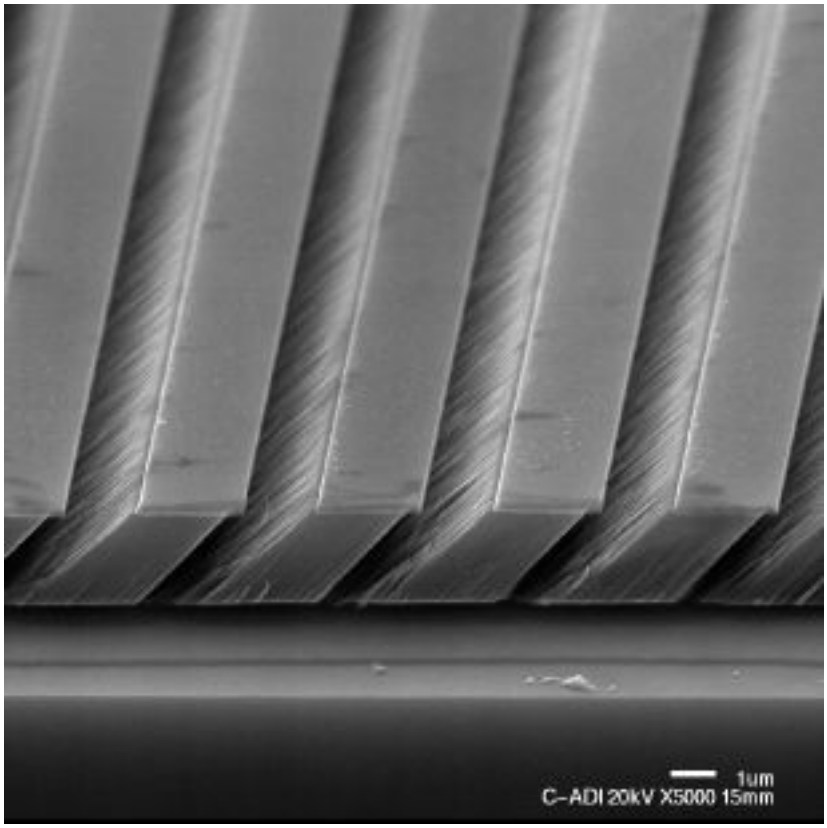

Figure 4.1. SEM picture of preliminary etching result of deep slanted grating using Atomic Oxygen Etching technique on polyimide material at Los Alamos National Laboratory [55].

Researchers at the Los Alamos National Laboratory have recently explored slanted grating fabrication using an Atomic Oxygen Etching (AOE) technique [55]. In AOE, to obtain the slanted profile with a high aspect ratio, a beam of atomic oxygen is highly collimated and the substrate is inclined at the desired slant angle during the etching process. Figure 4.1 is a SEM picture of a preliminary etch on a polyimide sample. Earlier processing steps before etching were done in our Nano and Micro Devices Center at the University of Alabama in Huntsville. A deep (over 1μm) grating with about a 45^0 slant angle was obtained. Further etching will be performed on high index material ($n \approx 2.0$).

Submicron and/or nano structures will be critical in the development of the next decade's communications infrastructure, and will certainly play a role in the next great leap forward in telecommunications. Although, so far, there has been no report of successful fabrication of submicron slanted gratings with high aspect ratios on high index material, we believe future progress in etching capability will make new types of semiconductor materials and devices possible.

4.2 SLGC simulation and design

Figure 4.2 is a 2D cross-sectional view of the SLGC and it is also the schematic geometry of the SLGCs simulated by 2D FDTD. The underlying 2D slab waveguide is a 1.0μm thick single mode waveguide with core and cladding refractive indices of 1.5073 and 1.46 respectively. The slanted grating is positioned on top of the waveguide core and embedded in the upper cladding of the waveguide. Silicon nitride (n=2.0 at a wavelength of λ_0=1.55μm) is used as the ridge material for the grating. The high index contrast

between the grating and waveguide materials together with a thick grating layer strongly disturbs the underlying waveguide mode in the coupling region. Because of this strong coupling mechanism, efficient coupling can occur with a short grating. The fiber we simulated is a single mode fiber with a core size of 8.3μm and core and cladding refractive indices of 1.470 and 1.4647, respectively. This fiber is simulated as a 2D slab waveguide. Berenger PML boundary conditions [31] are used to terminate and minimize the simulation region. The whole structure fits in an overall FDTD simulation area of 40μm×8μm. A square Yee cell of 36nm is used in both the x and y directions. We found that 7000 time steps are sufficient for the FDTD simulation to reach steady state. Note that only TE polarization (electric field out of the plane) is considered in this dissertation.

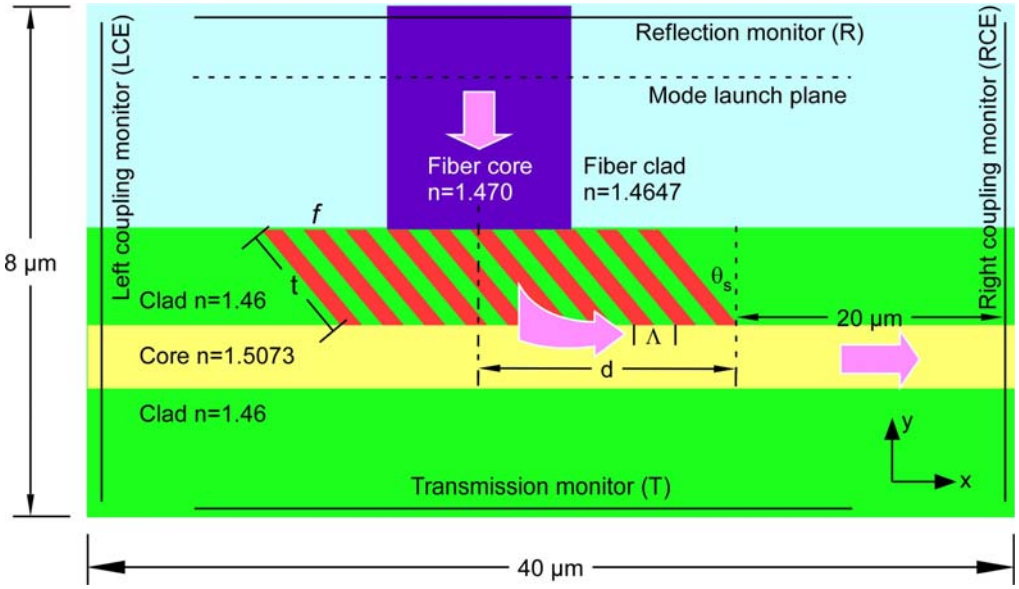

Figure 4.2. 2D cross-sectional geometry of SLGC used in the 2D FDTD simulation.

Parameters considered for maximizing the η_{RCE} (see definition in Chapter 3) of the SLGCs include grating period, Λ, in the x direction; the grating depth along the

slanted direction, t; the fill factor (grating ridge width/period), f; the slant angle, θ_s; and the relative lateral position between the fiber and the slanted grating, d.

4.2.1 Uniform SLGC

Let us first consider a simple SLGC, which we will call a uniform SLGC, which has a fixed fill factor for all of the grating ridges. For μGA optimization, the grating period, grating depth, fill factor, the slant angle, and the relative fiber/waveguide lateral position, are set as independent variables. Note that we change the period of the slanted grating during the optimization. As discussed in Chapter 3, this is required to meet the complicated phase-matching condition of the SLGC. With only five variables involved in the optimization, μGA converges very fast and gives us several designs with similar performance. Table 4.1 shows the variable ranges of μGA and the final optimized values for one of the designs.

The geometry of this particular uniform SLGC design is shown in Figure 4.3(a). Figure 4.3(b) shows the corresponding image plot of the magnitude squared of the time averaged electric field from 2D FDTD simulation. η_{RCE}, η_{LCE}, η_R and η_T are 66.8%, 0.69%, 6.63%, and 18.48% respectively. We can see several salient features of SLGCs from this design. First, with a grating period of 1.026μm, the slanted grating spans less than 20μm. It is well known that it is essentially impossible for traditional weak index-modulated grating couplers to achieve high coupling efficiency within such a short coupling length. Second, we notice that the slanted grating greatly suppresses the left coupled light. The left coupling efficiency (η_{LCE}) is only 0.69%, which demonstrates the excellent unidirectional coupling capability of the SLGC. It is also interesting to note that the power coupled toward the right without considering the mode overlap integral (i.e.,

just the power ratio term in Equation 3.1 in Chapter 3) is 74.2%. This means that 7.4% of the incident power (or 10% of the coupled power) radiates away from the waveguide along the propagation direction due to a mismatch between the monitored field and the waveguide mode. This loss originates from the mode mismatch between the coupled leaky mode and the output waveguide mode, and boundary scattering at the right edge of the slanted grating.

Table 4.1 μGA optimization of a uniform SLGC

Variables	Variable range	μGA optimized value
Grating period (μm)	0.5 – 3.0	1.026
Grating depth *t* (μm)	0.01 – 3.0	1.626
Fill factor *f* (%)	10 – 70	23.0
Slant angle θ_s (°)	1 – 90	34.98
Lateral position *d* (μm)	-10 – 10	6.300

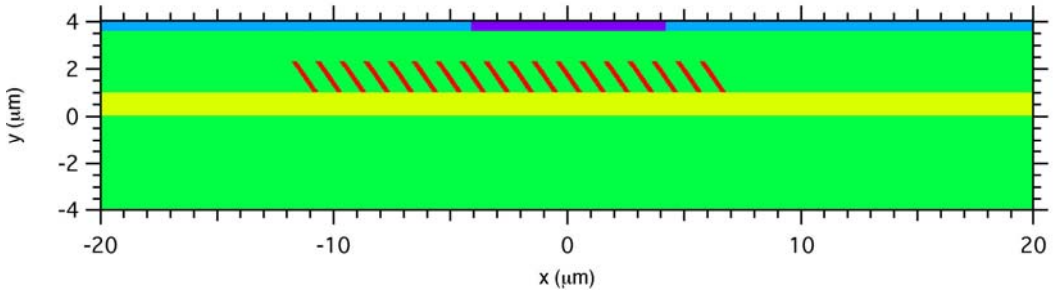

(a)

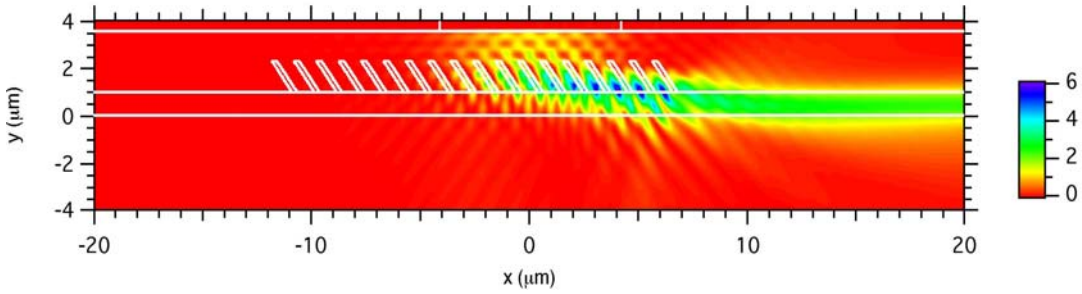

(b)

Figure 4.3. (a) Geometry of uniform SLGC optimized by μGA. (b) 2D FDTD result of magnitude squared time averaged E_z component for the uniform SLGC.

4.2.2 Non-uniform SLGC

In order to further improve the performance of SLGCs, non-uniform fill factor SLGC designs are considered. For this case, the fill factor of every grating ridge in the SLGC is independently changed. This idea is motivated by prism coupling, where it is possible to realize 100% coupling efficiency by varying the gap between the bottom side of the prism and the slab waveguide, which changes the local coupling coefficient [56]. For weak grating couplers, both varying the grating depth [10] and the fill factor [57] of

individual grating ridges has been studied to improve performance. For fabrication simplicity, here we investigate the non-uniform fill factor approach.

In μGA optimization of non-uniform SLGC, the fill factors of all 18 grating ridges are varied independently in the range of 10% to 90%. The ranges for all other variables are the same as those in the previous uniform SLGC case. Therefore 22 variables are optimized and approximately 400-500 generations are required for μGA to converge to a reasonable design. Figure 4.4(a) shows the geometry of an optimized non-uniform SLGC. Figure 4.4(b) is an image plot of the magnitude squared time average electric field.

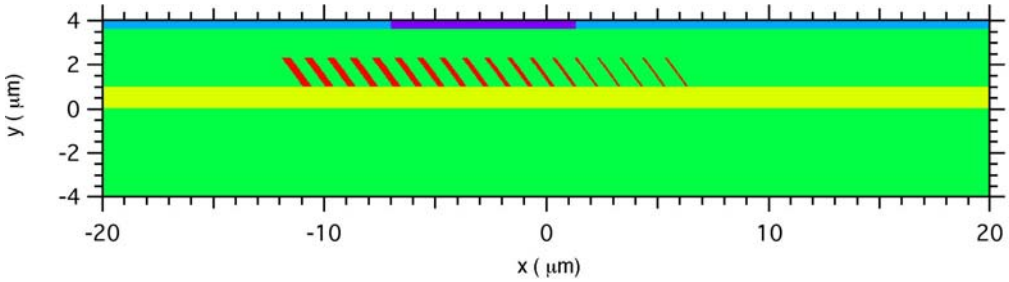

(a)

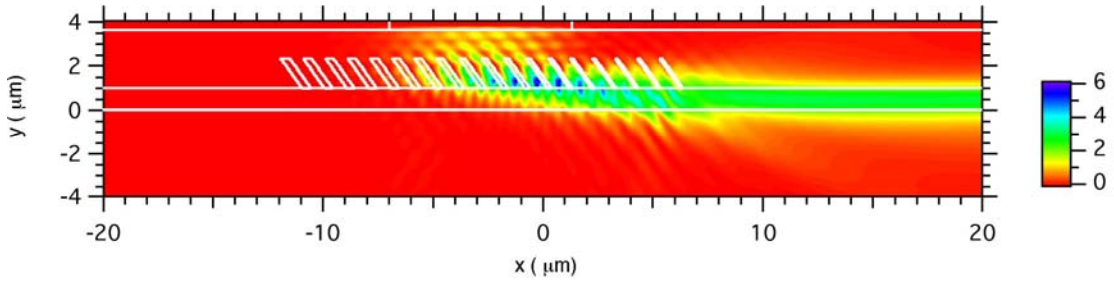

(b)

Figure 4.4(a) Geometry of non-uniform SLGC optimized by μGA. (b) 2D FDTD result of magnitude squared time averaged E_z component for the non-uniform SLGC.

The optimized SLGC parameters are Λ =1.013μm, t=1.627μm, θ_s=35.94^0, and d= 10.12μm. These values are very close to those of uniform SLGC except the lateral position d of the incident fiber. This SLGC has a right coupling efficiency (η_{RCE}) of 80.1%, which is 13% greater than the uniform SLGC design. The improvement mainly comes from the decrease of the transmitted light (η_T) to the substrate, which is 10.04%. Efficiency of η_R and η_{LCE} also decreased to 4.02% and 0.19% respectively.

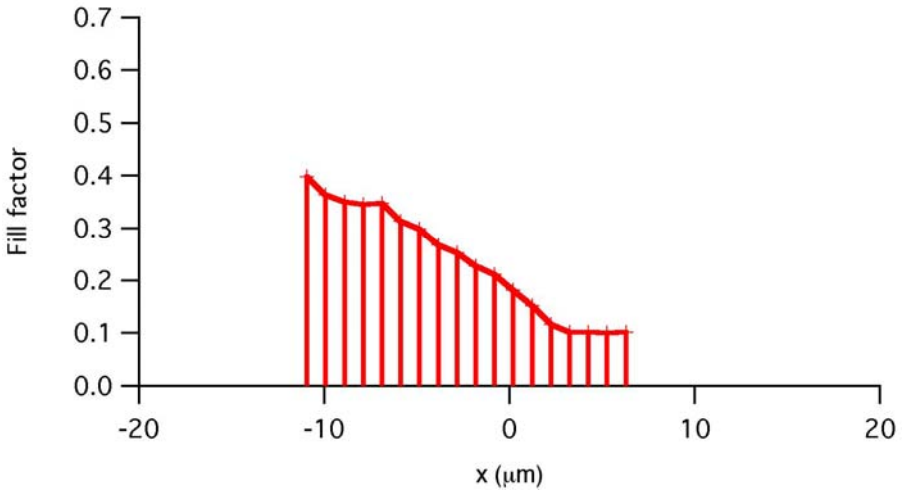

Figure 4.5. Fill factor distribution of μGA optimized grating along x direction for non-uniform SLGC shown in Figure 4.4.

Figure 4.5 illustrates the μGA optimized fill factor as a function of the ridge position in the x direction. It is clear that the fill factor of the grating ridges gradually decreases along the coupling direction. The fill factors of the four right-most grating ridges are essentially at the lower allowable limit used in the μGA optimization. However, the average fill factor of all of the grating ridges is 23.48%, which is almost the same as that of the uniform case. Notice that the incident fiber is also pushed to the left

compared to the uniform SLGC design. The locally varied fill factor profile causes a redistribution of the field inside the coupling region to minimize the reflected, transmitted and scattered light, which in turn results in better performance.

4.3 Physical analysis and discussion

We use the same RCWA method as in Chapter 3 to solve the so-called homogeneous problem [38] for SLGCs for the complex propagation constants $\gamma_m = \beta_m + i\alpha_m$ (m is the mode index) of the leaky modes supported by the SLGC. To apply RCWA, not only the proposed finite length SLGCs have to be infinitely extended in the x direction, but also the SLGCs must be divided into multiple sub-layers in the y direction in order to model the sloped ridge of the SLGCs with RCWA, as illustrated in Figure 4.6.

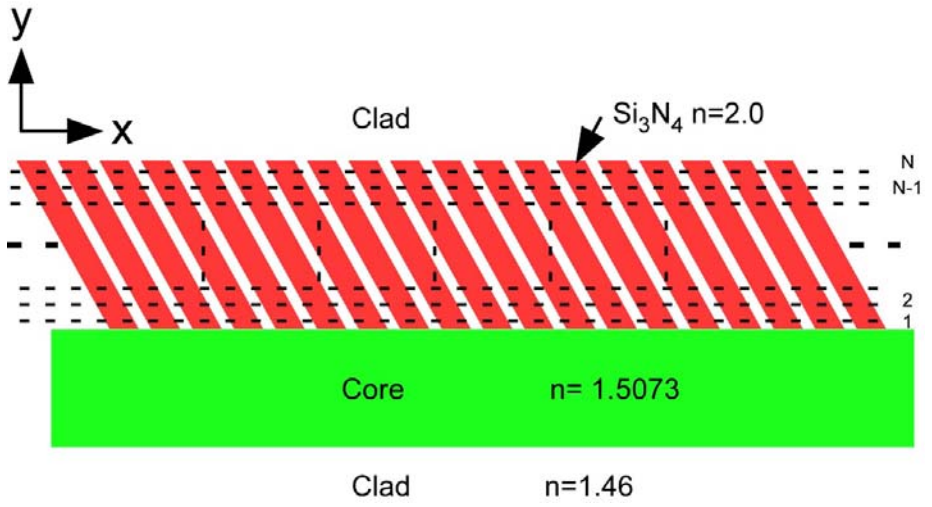

Figure 4.6. Infinite periodic version of the SLGC for leaky mode calculation with RCWA approach.

First we examine the leaky modes of the uniform SLGC design discussed in Section 4.2.1. The 1.626μm deep slanted grating layer is divided into 100 sub-layers in the RCWA mode analysis. At λ=1.55μm, the two lowest-order leaky modes are the fundamental mode with $\gamma_0=\beta_0+i\alpha_0$=6.1220+i0.3196 and an effective index of 1.5102, and a higher order mode with $\gamma_1=\beta_1+i\alpha_1$= 6.0268+i0.0465 and an effective index of 1.4867. The presence of the grating increases the effective waveguide thickness sufficiently to allow a higher order leaky mode to exist in addition to the fundamental leaky mode. The slab waveguide (i.e., the region without the SLGC) supports a single mode with an effective index of 1.4760, which is very close to the effective index of the higher order leaky mode (1.4867).

Equipped with accurate mode effective index information, we can now investigate the phase match condition of this uniform SLGC as shown in Figure 4.3. Using the phase match condition for normal incidence, with a μGA optimized grating period of Λ=1.026μm, it is straightforward to show that the phase match condition of the uniform SLGC can be satisfied with the fundamental leaky mode through the +1 diffraction order of the grating. Since there is a discontinuity in the effective index (or phase velocity) at the grating boundary between the fundamental leaky mode and the slab waveguide mode, both scattering loss and reflection can take place at the boundary. It is interesting to note that although the effective index of the higher order leaky mode and the slab waveguide are similar to each other, the μGA optimization selects the fundamental leaky mode instead. If the phase match condition was met through the higher order leaky mode, scattering loss and reflection at the boundary could be minimized. One reason for this outcome is the difference in the radiation factor α between the fundamental leaky

(α=0.3196) and higher order leaky mode (α=0.0464). The larger α of the fundamental leaky mode ensures high efficiency coupling within a short coupling length that is close to incidence beam size [11].

As shown in Figure 4.7, a k-vector diagram is a very useful aid in understanding the operation of SLGCs. As a zeroth order approximation, the slanted grating layer of the SLGC can be treated as a homogeneous layer with an effective index defined as the volume average between the two materials forming the grating [46] [47] [52]:

$$n_{eff} = \sqrt{n_1^2 \times fillfactor + n_2^2 \times (1 - fillfactor)} \quad , \tag{4.1}$$

The solid circle with a radius of 1.6004 denotes the average refractive index of the grating layers. The incident k-vector is $\vec{k}_{inc}$ and the dashed slanted line refers to the orientation of a slanted fringe at 34.78° relative to the k_y axis. The two dashed vertical lines L_1 and L_2 at k_x = 1.4760 and 1.5102 correspond to the effective indices of the slab waveguide mode and the fundamental leaky mode, respectively. The first diffraction order $\vec{k}_{final}$, which is the vector sum of the grating vector $\vec{K}_G$ and $\vec{k}_{inc}$, is found to terminate at the intersection point C between the solid circle and the vertical line L_2, which means that the Bragg diffraction condition is satisfied simultaneously with the phase matching condition. Bragg diffraction tends to suppress all but the +1 diffraction order and therefore enforces unidirectional coupling into the waveguide. For surface-normal operation, the occurrence of Bragg diffraction is the main advantage of an asymmetric grating shape compared to a symmetric grating.

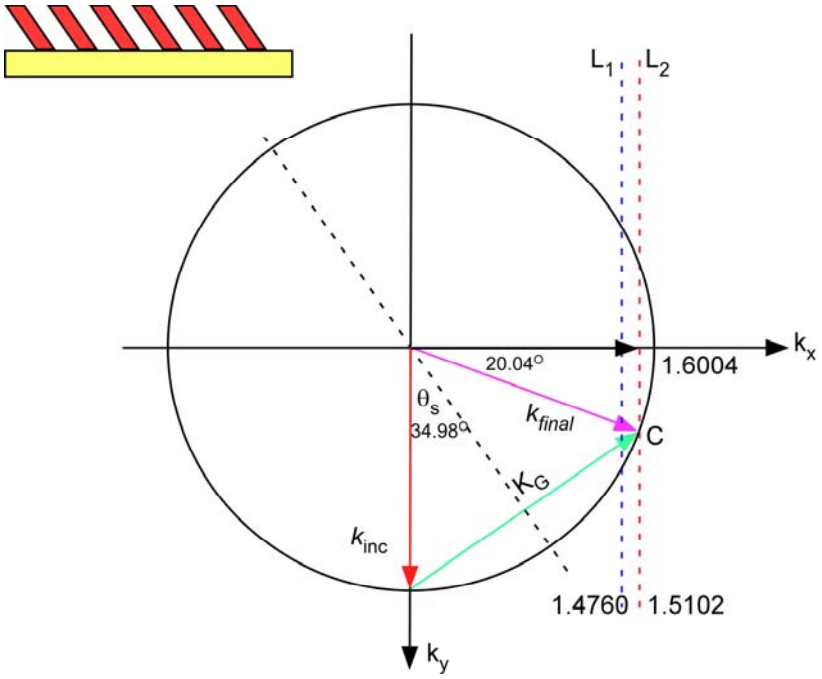

Figure 4.7. k-vector diagram of the uniform fill-factor SLGC presented in Section 4.2.1, the inset shows the slanted grating.

It is interesting that the direction of $\vec{k}_{final}$ in Figure 4.7 is tilted at about 20° with respect to the k_x axis. This implies that the phase front in the SLGC coupling region for the structure of Figure 4.3 should also be tilted about 20° with respect to the x-axis. The tilted phase front can be clearly seen from an image plot of the phase distribution of this SLGC calculated by 2D-FDTD, which is shown in Figure 4.8. Colors indicate constant phase fronts.The tilted wavefront is quite flat when the light is coupled in by SLGC and is gradually rippled in the area around the right end interface of the slanted grating. The tilted wave front and the mismatch between the effective indices of the waveguide mode and the fundamental leaky mode of SLGC (the distance between L_1 and L_2 as shown in Figure 4.7) will induce scattering loss at the boundary between the slanted grating region

and the undisturbed waveguide region. In general this scattering loss is more severe than that of grating couplers that operate in the weak coupling regime where the mode mismatch is assumed to be negligible.

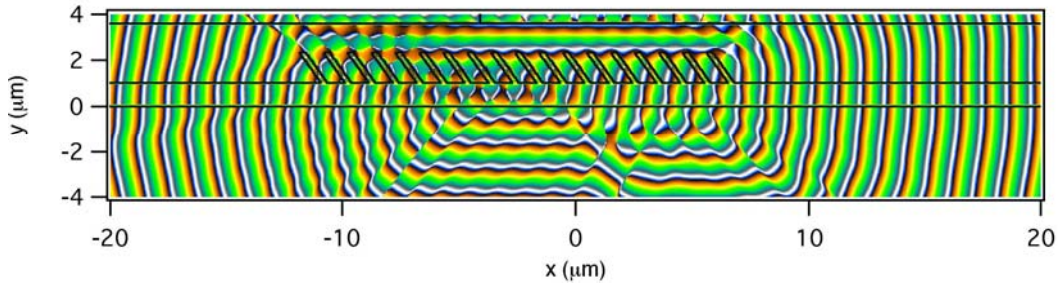

Figure 4.8. Phase distribution from 2D FDTD simulation on the uniform SLGC.

The above RCWA mode analysis procedure explains the behavior of the μGA-optimized uniform SLGC. Nevertheless, it cannot be directly applied to the analysis of the non-uniform SLGC discussed in Section 4.2.2 because of the varying fill factor of the grating ridges. In order to apply a similar mode analysis, the non-uniform SLGC is first approximated as a uniform SLGC with a fill factor of 23.48%, which is the average of the fill factors of all of the grating ridges. For this simplified SLGC, two leaky modes can be found with RCWA mode analysis: a fundamental mode with propagation constant $\gamma_0=\beta_0+i\alpha_0$= 6.201752 + 0.3148340i (n_{eff}=1.5299) and a higher order mode with $\gamma_1=\beta_1+i\alpha_1$= 6.029924 + 0.040366i ($n_{eff}$= 1.4875). It is straightforward to show that both the phase-matching and Bragg conditions are satisfied for the fundamental leaky mode. The k-vector diagram and the phase distribution of the 2D FDTD simulation are shown in Figures 4.9(a) and (b), respectively. Although these figures are very similar to those for the uniform SLGC case, we notice that the phase ripple near the right hand termination of

the grating in Figure 4.9(b) is much less than in Figure 4.8, which means that the transition from the coupling grating to the output waveguide is smoother and hence the scattering loss is lessened.

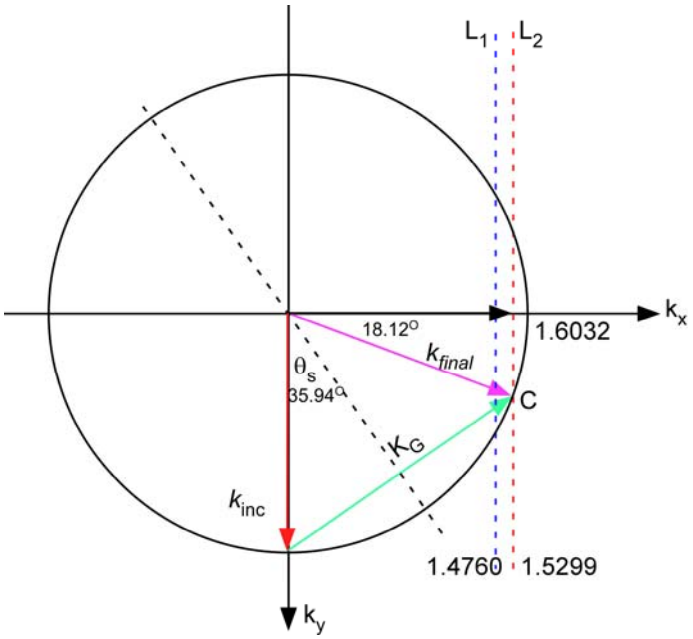

(a)

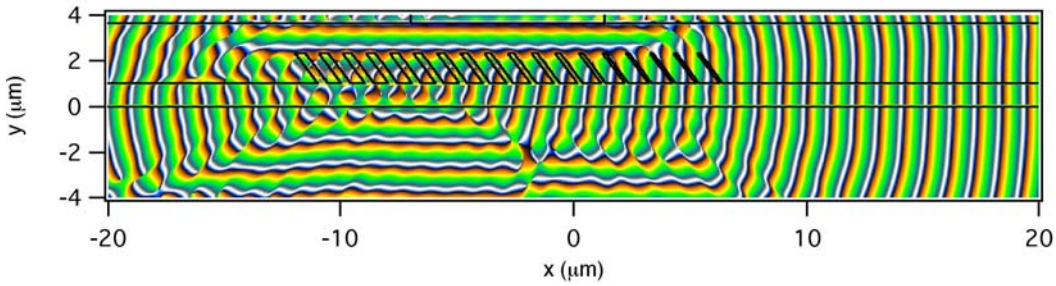

(b)

Figure 4.9. (a) k-vector diagram of non-uniform SLGC. (b) 2D FDTD Phase distribution of the non-uniform SLGC.

Further 2D FDTD simulation reveals that the SLGC design has performance similar to SWGC, namely a relaxed lateral fiber alignment tolerance and a relatively broad spectral response. Figure 4.10 and Figure 4.11 show the results for nonuniform SLGC. On both plots, the triangle points are those simulated by FDTD. These features may be attractive for many photonic systems.

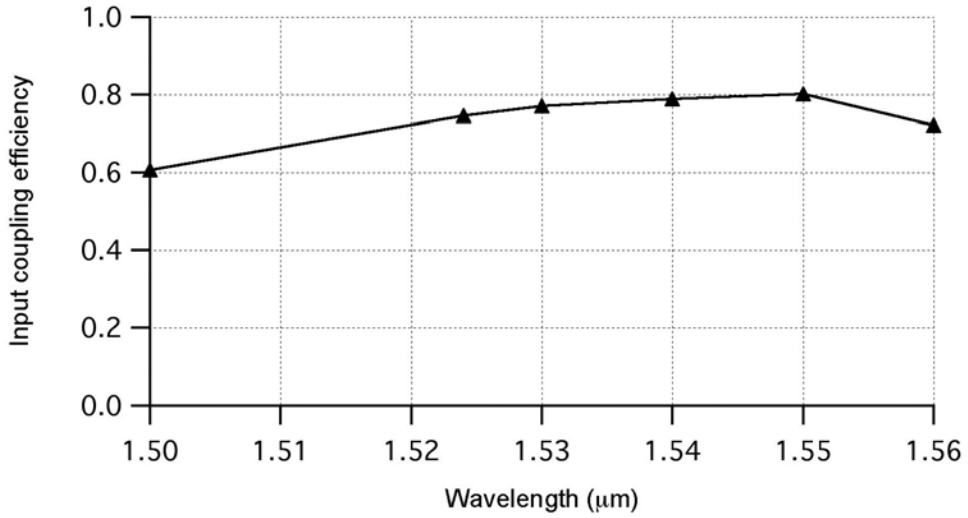

Figure 4.10. 2D FDTD simulated spectral response of the non-uniform SLGC design.

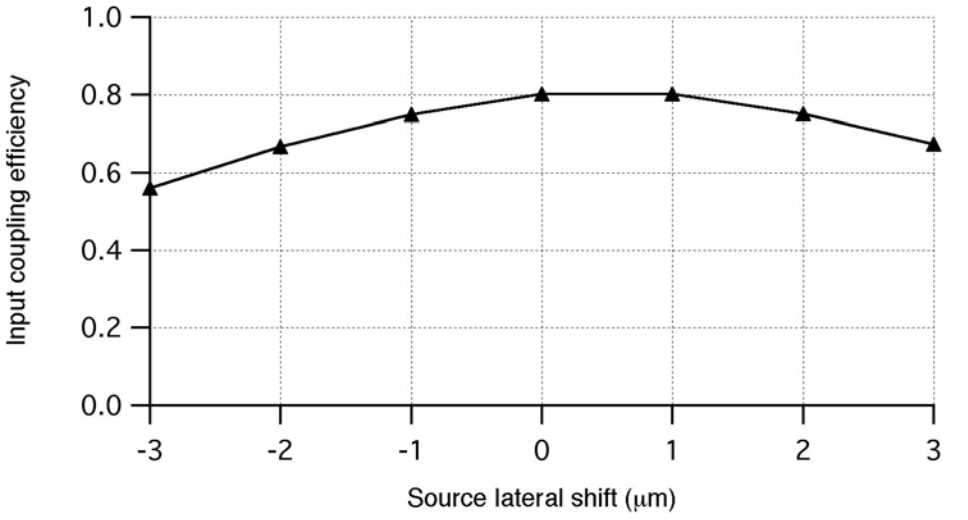

Figure 4.11. Fiber lateral shift sensitivity analysis of the non-uniform SLGC design.

Finally, there is one more point worth mentioning. In both the SLGC design discussed above and the SWGC in chapter 3, we found that they can support a higher order leaky mode in addition to the main fundamental leaky mode. It seems that SLGCs/SWGCs generally support multiple leaky modes because of the introduction of a high index material as the grating ridge for strongly coupled SLGCs/SWGC. It is well known that alternative leaky channels are not desirable in traditional weak grating couplers. However, as demonstrated by these μGA-optimized SLGCs/SWGCs, if properly designed, the higher order mode will be greatly suppressed and therefore its presence will not appreciably affect the performance of SLGCs/SWGCs.

4.4 Fabrication tolerance

Further FDTD simulations were performed on uniform grating couplesr in Section 4.2.1 to access the tolerance for the grating structures for fabrication. The criterion for the tolerance is that the coupling efficiency is maintained greater than 60%. The tolerance for the slanted angle is about ±4° which is more relaxed than slanted gratings at the Bragg angle for weak coupling. Grating length and ridge width tolerances are 200nm and 100nm, respectively.

4.5 Output coupler

In weak grating coupling, following reciprocity arguments, any grating designed to serve as an input coupler can also be used as an output coupler [9] [10] [11]. In order to prove this reciprocal relationship, which is also applicable to our strong grating coupling, the input couplers designed in Sections 4.2.1 and 4.2.2 are simulated as output

couplers. The fundamental mode of the waveguide is sourced at the right side of the FDTD simulation region as incidence and propagates toward the grating coupler and is coupled out into the fiber waveguide on top. The image plots of the magnitude of the time averaged E_z component and phase distribution from FDTD simulation are shown in Figures 4.12 and 4.13 for uniform and non-uniform SLGC, respectively. In this case, the output beam emitted from the output coupler should propagate along the +y direction opposite the incident propagation for the input coupler. Figures 4.12(b) and 4.13(b) clearly show that the phase front coupled out is parallel to the x-axis which means the wave propagation is along the +y direction. Further coupling efficiency calculations with mode overlap integrals have shown that the output coupling efficiency is 66.2% and 80.4% for uniform and non-uniform output couplers, respectively, which is very close to the corresponding input coupling efficiency considering the calculation error.

By reciprocity, an analysis of the output coupler may give us more insight into the mechanism of the input coupler. It is recognized that the output profile emitted from a uniform grating output coupler is a decaying exponential. Figure 4.14(a) shows the cross section of the near field pattern of the magnitude of the time averaged E_z component in Figure 4.12(a). The right edge of the slope and the ripple oscillation may be due to an edge effect caused by diffraction. The fiber mode has typically a Gaussian-like profile; however, this fundamental mismatch prevents higher coupling efficiency for a uniform grating output coupler or input coupler. This suggests that a Gaussian beam profile from the output coupler is desirable and this can be achieved by using a grating structure varying along the guiding direction. In practice it is much easier to change the grating fill factor using high resolution e-beam lithography. Compared to Figure 4.14(a),

Figure 4.14(b) shows a more-Gaussian like profile. We found, for the uniform output coupler, there is about 74% of total power coupled out by the grating. By including mode overlap integral, about 89% of the output power is guided by the fiber waveguide as the fundamental mode. For the non-uniform output coupler, about 87% of the total power is coupled out by grating. About 92% percent of this power is really guided by the fiber waveguide as fundamental mode. Since the beam size and the number of grating periods are limited, the improvement in coupling efficiency for the Gaussian profile match is less than the weak coupling case where the beam size is assumed infinity. However, since the mode transition from the waveguide to the coupling grating (or coupling grating to waveguide for an input coupler) is smoother and the reflectance and scattering is lessened. Therefore, more light is coupled into the waveguide (without the grating) eventually.

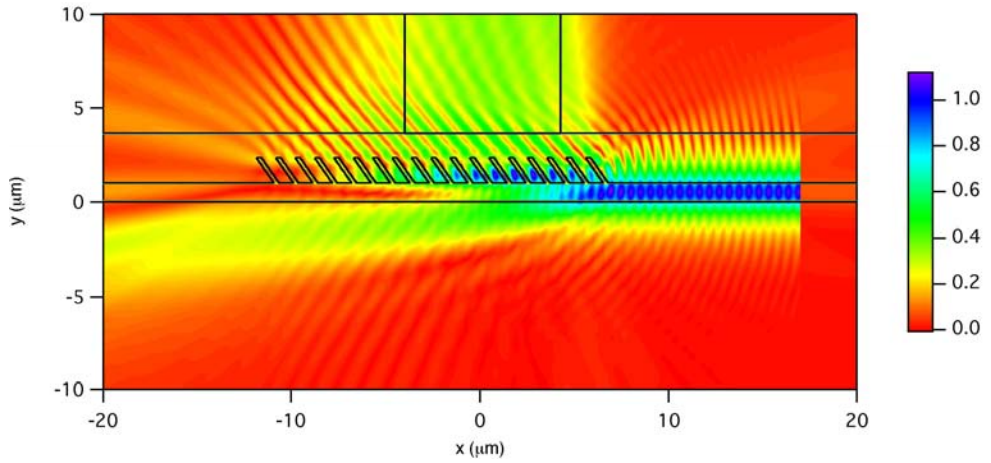

(a)

Figure 4.12. (a) Image plot of magnitude time averaged E_z components from FDTD simulation of the uniform SLGC as an output coupler.

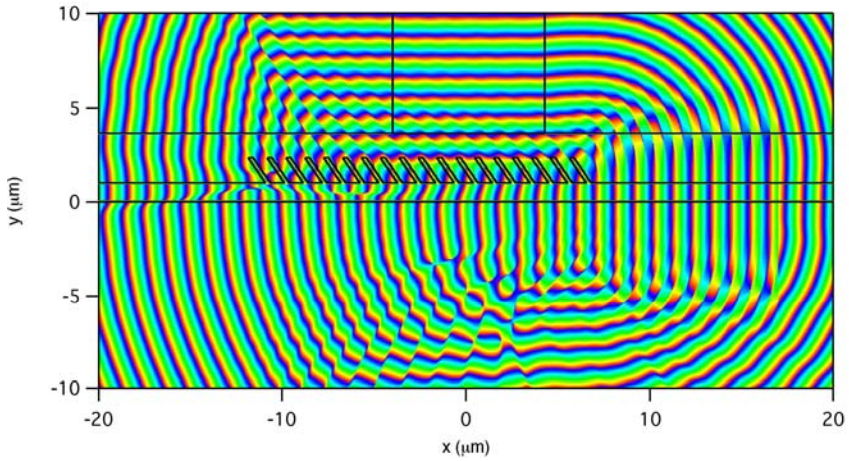

(b)

Figure 4.12. Continue (b) Phase distribution from FDTD simulation of the uniform SLGC as an output coupler.

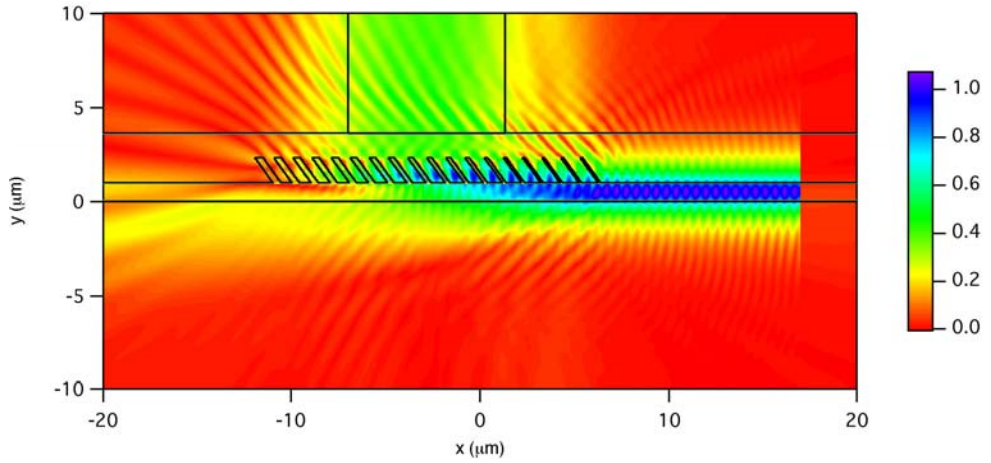

(a)

Figure 4.13. (a) Image plot of magnitude time averaged E_z components from FDTD simulation of the non-uniform SLGC as an output coupler.

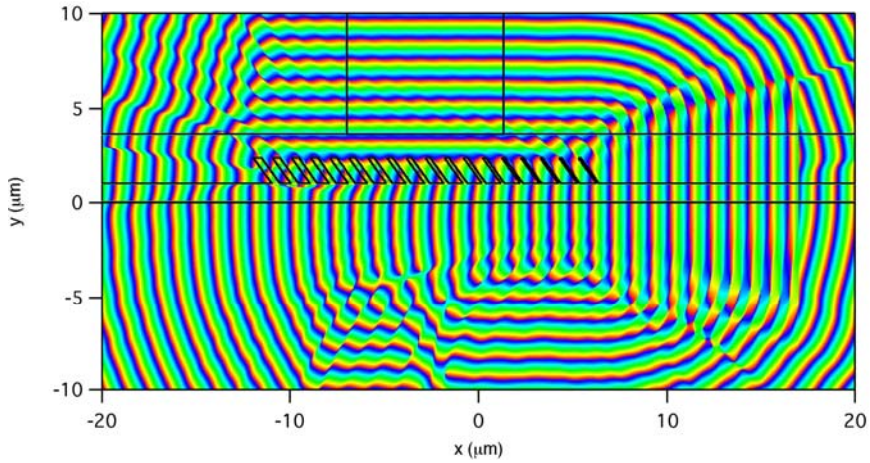

(b)

Figure 4.13. Continue (b) Phase distribution from FDTD simulation of the non-uniform SLGC as an output coupler.

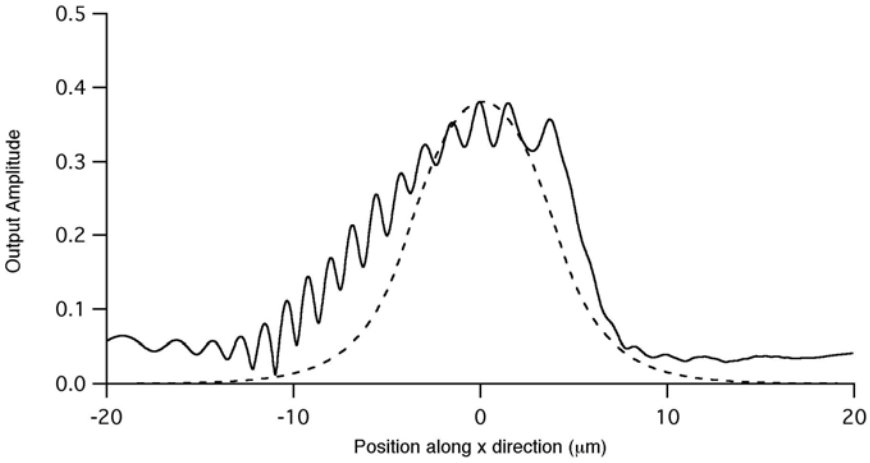

(a)

Figure 4.14. A cross section of the near field amplitude of (a) the uniform output coupler. For comparison, the profile of fiber mode is overlapped on the plots as a dotted line.

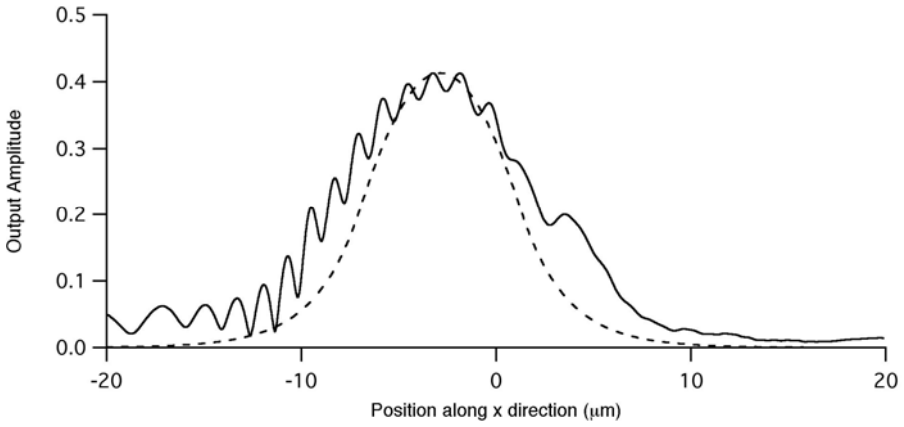

(b)

Figure 4.14. Continue of (b) the non-uniform output coupler. For comparison, the profile of fiber mode is overlapped on the plots as a dotted line.

4.6 Conclusions

In this chapter, we proposed the utilization of strong index-modulated slanted grating couplers (SLGCs) as a potential coupler technology for surface-normal coupling between fibers and waveguides for dense PLCs. The major advantage of our SLGCs is that they can realize high efficiency unidirectional coupling for surface-normal operation in a very short coupling length, i.e., on the order of the width of a fiber mode. With the help of a powerful μGA-2D FDTD design tool, highly efficienct SLGCs, both uniform and non-uniform, have been designed.

Rigorous mode analysis shows that the phase-matching mechanism of SLGCs is different from the traditional grating couplers with weak index modulation. Both the phase-matching and Bragg conditions are satisfied with respect to the fundamental leaky

mode of the SLGCs instead of the output waveguide mode. 2D FDTD simulation also shows that SLGCs have a large tolerance for lateral fiber misalignment and a broad spectral response. Such grating couplers, taking advantage of planar processing, can offer the potential to surmount the difficulties typically associated with coupling from fibers oriented normally to a waveguide surface. By reciprocal relationship between input coupler and output coupler, calculating the output field gives us more insight into the physics of input couplers, particularly non-uniform input couplers, when the optimized input couplers are used as output couplers.

Chapter 5

EMBEDDED SLANTED GRATING

In Chapters 3 and 4, the grating is positioned on the top of the single mode slab waveguide. In this chapter, we propose an embedded slanted grating coupler (ESGC) for the same application—vertical coupling between optical fibers and planar waveguides. A grating with a parallelogram shape is designed to be embedded through the entire high-index waveguide core. Simulations are first performed for a 240nm thick silicon-on-insulator (SOI) planar waveguide. It shows that up to 75.8% coupling efficiency can be obtained between a single mode fiber and a 240nm thick SOI planar waveguide. FDTD simulation results are also presented based on waveguide material simulated in Chapters 3 and 4, with a core refractive index of n_1= 1.5073 embedded in a cladding with n_2=1.4600 (refractive index contrast Δ=3.1%).

5.1 Introduction

In ESGC, the slanted grating is moved into the waveguide core and completely embedded in the high index core material. This provides advantages. First, this can achieve full volume interaction between the grating and the waveguide mode, in contrast to the SLGC and SWGC that has modulation only on the top of waveguide core. It is

especially suitable for a high index contrast waveguide like SOI in which light is strongly confined in a waveguide core layer of a few hundred nanometers in transverse dimension. Secondly, the field distribution in the grating region of the ESGC is centered within the waveguide, which improves the mode transition from the grating region to the non-grating region and thus reduces scattering loss at the boundary. There are additional advantages that depend on the specific waveguide core material. In the SOI waveguide, the etched grooves in an ESGC have an aspect ratio near 1, which is much smaller than that required for an SLGC.

5.2 ESGC simulation and design based on the SOI waveguide

5.2.1 Simulation results

Figure 5.1 schematically illustrates the geometry of an ESGC. The grating is embedded within the waveguide core region with an overlying upper cladding that fills the grating grooves. The single-mode planar waveguide is a 240nm-thick core layer of Si with refractive index 3.4. The lower cladding of SiO_2 has a refractive index of 1.4440, and it is assumed to be thick enough so that no light is coupled into the Si substrate. The upper cladding is assumed to have a refractive index of 1.4600.

The core and cladding refractive indices are 1.4840 and 1.4600 respectively. As shown in Figure 5.1, the source of the fundamental mode of the fiber waveguide is at the top of the FDTD simulation region, propagates to the right toward the grating coupler and is coupled into the waveguide. In order to save simulation time, we first use a coarse square Yee cell of 10nm x 10nm. After a suitable result is found, the Yee cell is

decreased to 3nm and 6nm in the x and y directions, respectively, to fine tune and verify the coarse design. Note that only TE polarization (electric field out of the plane) is considered in this chapter. All simulations are performed for λ=1.55μm.

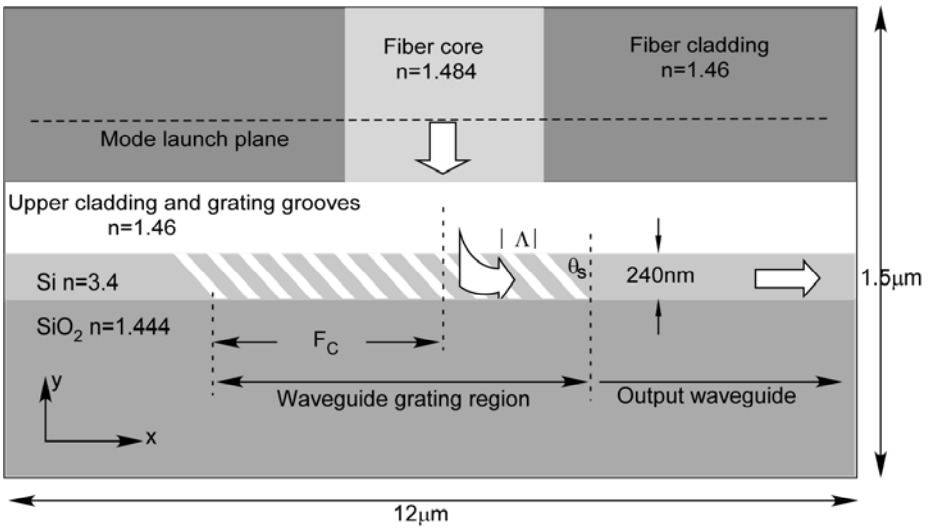

Figure 5.1. Schematic diagram of ESGC geometry.

During μGA optimization, the independent variables are the grating period along the x-direction Λ, the fill factor f (which is the ratio of the low index grating ridge width to the period), the slant angle θ_s (relative to waveguide normal), and the lateral distance, F_c, between the center of the fiber and the left edge of the bottom of the grating.

First, the same single mode fiber used in the simulations in Chapters 3 and 4, which was based on Corning's SMF-28 single mode optical fiber, is considered (with a core size of 8.3μm and core and cladding indices of 1.4700 and 1.4647, respectively). The entire computational structure for the FDTD simulation has an overall area of 30μm×1.5μm which covers 20 periods of the grating structure to fit the fiber size. Figure 5.2 shows an image plot of magnitude squared time averaged electric field of the

μGA optimized ESGC overlapped with the ESGC geometry for Λ=0.632μm, θ_s=60.9^0 and F_c=9.09μm. Note that the vertical and horizontal dimensions are not drawn to scale for a clearer view, for the SOI waveguide cases throughout this chapter.

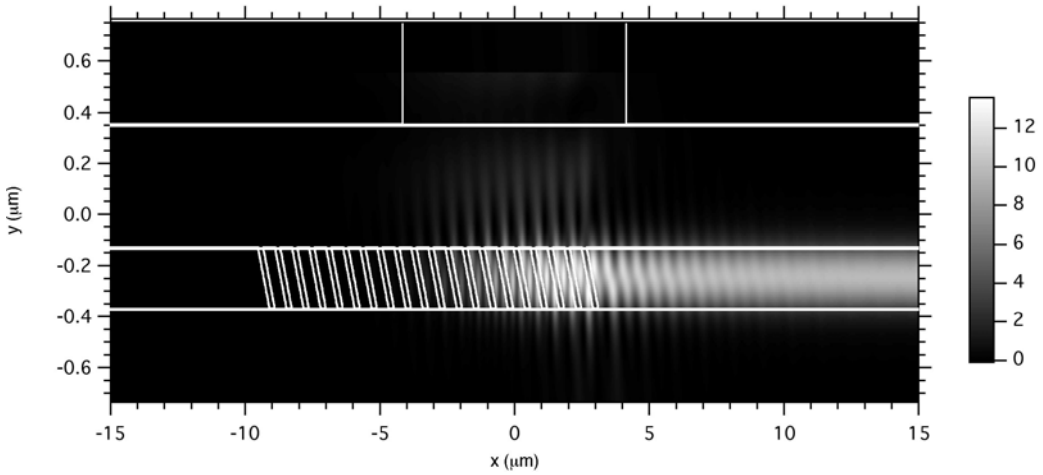

Figure 5.2. Image plot of magnitude squared time averaged E_z component from the FDTD simulation for the uniform ESGC with a fiber having a core size of 8.3μm.

The coupling efficiency is 64.5%. In Figure 5.2, we see that some of the light incidence on the right side is not launched into the grating but transmitted or reflected by the waveguide directly. This light is counted in the coupling loss. In Section 4.5 of the previous chapter, we proved the reciprocal relationship between input coupler and output coupler. It is recognized that the optimal input/output coupling can only be achieved if the output beam profile from output coupler (being used as input coupler as well) matches the Gaussian-like profile of the fiber mode. Figure 5.3(a) shows the magnitude time averaged E_z component from the FDTD simulation when the input coupler in Figure 5.2 is used as an output coupler. Figure 5.3(b) shows the cross section profile of

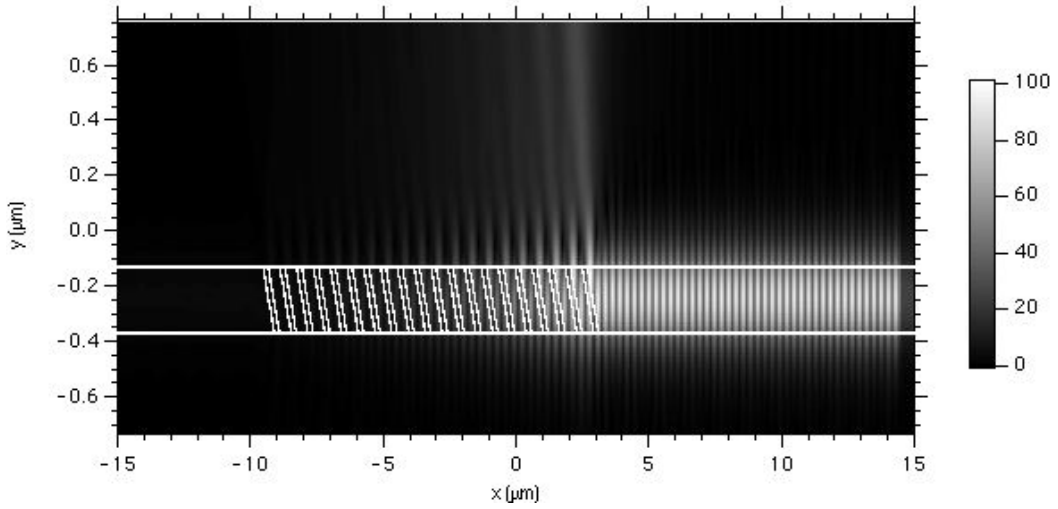

(a)

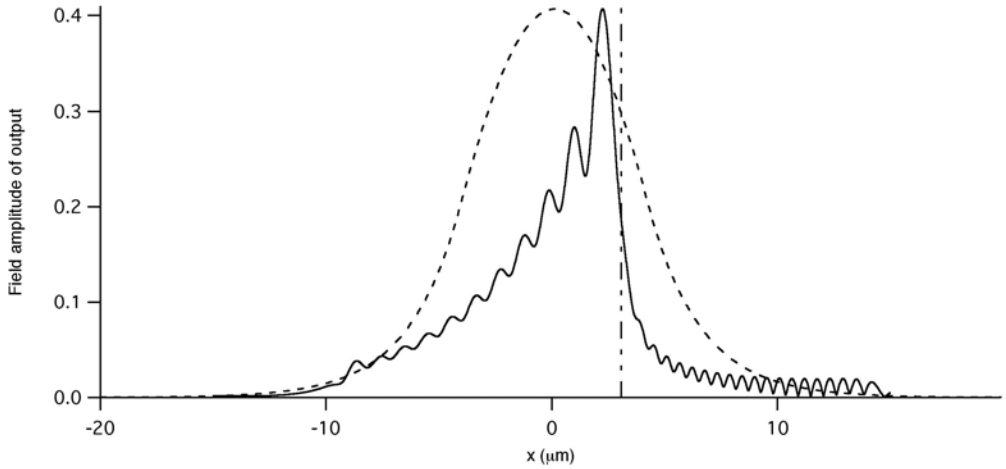

(b)

Figure 5.3. (a) Image plot of magnitude time averaged E_z component from the FDTD simulation when the input coupler in Figure 5.2 is used as an output coupler. (b) Cross section profile of near field of the output beam in Figure 5.3(a) with fiber mode profile (the dotted line) for comparison. The vertical dashed line shows the grating boundary at the right side.

near field of the output beam with fiber mode profile (shown as dotted line) for comparison. The vertical dashed line represents the right edge of the grating, and illustrates the portion of light from the fiber which is not incident on the grating. During the optimization process, μGA selected the best relative position between fiber and grating to optimize the mode match. Since the size of the fiber mode is much larger than that of the output beam, as shown in Figure 5.3(b), it turns out that the centers of the output beam and fiber mode are not coincident anymore.

In order to avoid the additional light loss for the fiber size mismatch, we exploited the fiber with smaller core size used in reference [8] focusing on taper coupling (edge coupling), which corresponds to a typical Erbium-doped optical fiber with core size of 4.4 μm and core and cladding indices of 1.4840 and 1.4600, respectively. The interesting thing is, in reference [8], the waveguide material is also silicon-based. The adoption of a smaller fiber size facilitates light coupling into a small waveguide. On this point, the taper coupler and grating coupler are similar.

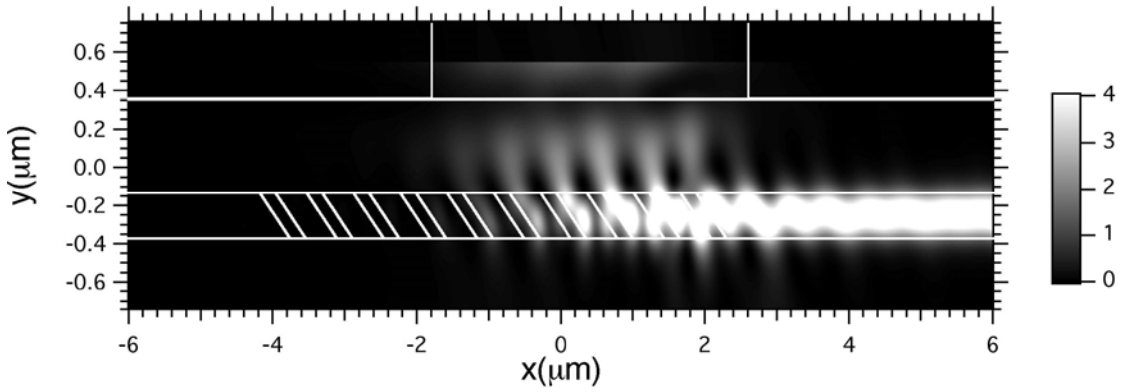

Figure 5.4. Image plot of magnitude squared time averaged E_z component from FDTD simulation on the uniform ESGC for a fiber with a core size of 4.4μm.

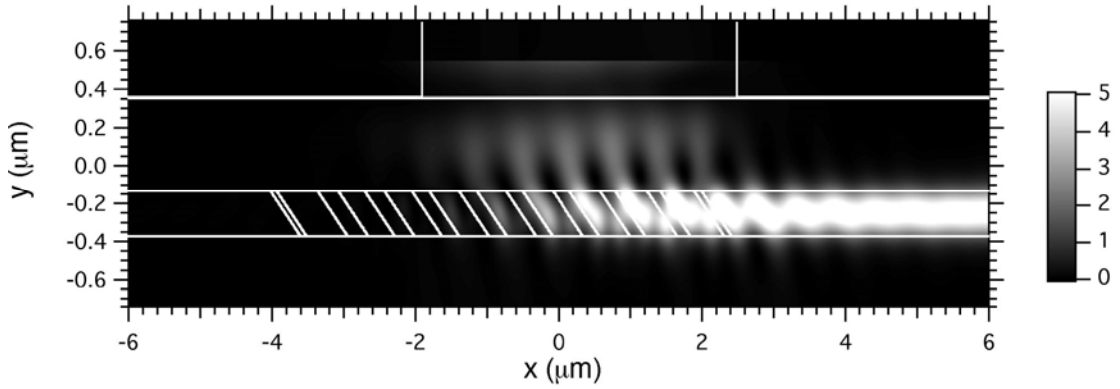

(a)

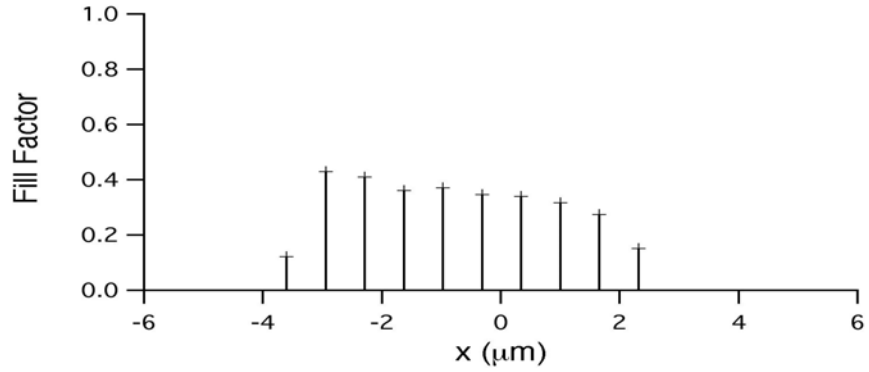

(b)

Figure 5.5. (a) Image plot of the magnitude squared time averaged electric field simulated by 2D FDTD for a fiber with a core size of 4.4μm. (b) Fill factor distribution of the non-uniform ESGC in (a).

The entire structure fits in an overall FDTD simulation area of 12μm×1.5μm with 10 grating periods. The magnitude squared time averaged electric field of the μGA optimized ESGC is shown in Figure 5.4 along with the ESGC geometry. Note that the vertical and horizontal dimensions are not drawn to scale. The corresponding Λ, f, θ_s and F_c are 0.6495μm, 0.328 (the groove width is 213nm), 59.71^o and 4.28μm, respectively. A

mode overlap integral calculation shows that the coupling efficiency for this optimized ESGC is 69.8%. Note that with a grating period of 0.6495μm and 10 periods, the grating spans less than 7μm.

To further improve the performance of ESGCs, we have also considered non-uniform fill factor [57] designs. In the μGA optimization of non-uniform ESGCs, the fill factors of all 10 grating periods are varied independently within the range of 10% to 90%. The optimized ESGC parameters are Λ=0.6573μm, θ_s=60.35^0 and F_c=3.9μm. The coupling efficiency is improved to 75.8%. Figure 5.5(a) shows the magnitude squared time averaged electric field and Figure 5.5(b) shows the μGA optimized fill factor as a function of the ridge position in the x direction.

Further 2D FDTD simulation reveals that ESGC design has a performance similar to SWGC and SLGC, namely a relatively broad spectral response as shown in Figure 5.6.

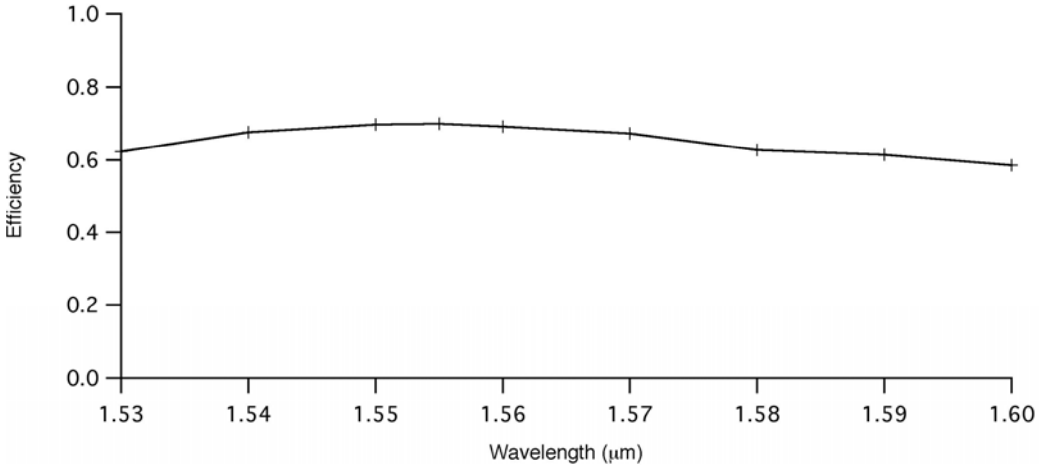

Figure 5.6. 2D FDTD simulated spectral response of the non-uniform ESGC design.

5.2.2 Discussion

We now investigate the physical operation of the μGA optimized ESGC. First we investigate the phase-matching condition. We substitute the optimized period Λ =0.6495μm and a wavelength of 1.55μm into Equation 3.2, and obtain n_{eff}=2.3864. A simple mode calculation shows that the effective index of the fundamental mode of the output waveguide (without grating) is 2.8340. Therefore it is obvious that the phase match is not satisfied with respect to the fundamental mode of the output waveguide.

On the other hand, a rigorous leaky mode analysis [48] of the ESGC reveals that the grating region has a fundamental leaky mode with an effective index of 2.3972. Note this is very close to the n_{eff} required by the phase matching condition. The slight difference of 0.0108 in index value is due to FDTD Yee cell discretization error. To show this, we take the derivative of Equation 3.2,

$$\delta n_{eff} = (\lambda_0 / \Lambda^2)\delta\Lambda, \tag{5.1}$$

and set $\delta\Lambda$ equal to 3nm (the Yee cell size) which gives δn_{eff} = 0.0110. The above index difference is within this error. Thus we conclude that, in ESGC, the phase matching condition is satisfied with respect to the fundamental leaky mode in the grating region through the +1 diffraction order of the grating.

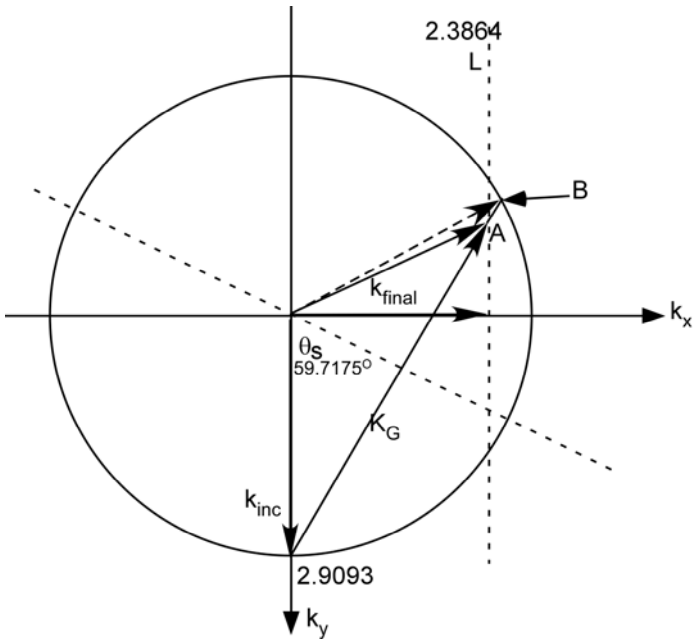

Figure 5.7. k-vector diagram of ESGC.

To study Bragg diffraction, we construct a k-vector diagram as shown in Figure 5.7. Note that all k vectors in the figure are normalized by k_0, the free space k-vector. The solid circle has a unitless radius of 2.9093 and denotes the average refractive index of the grating layer (see Equation 4.1 in Chapter 4). The dotted slanted line refers to the orientation of the slanted grating ridges relative to the k_y axis, which is 59.71° in this case. The dotted vertical line, L at k_x = 2.3864 corresponds to the effective index of the fundamental leaky mode. $\vec{k}_{inc}$ is the normal incident k-vector and $\vec{K}_G$ is the grating vector perpendicular to the orientation of the slanted ridges. The diffracted k vector, $\vec{k}_{final}$, which is the vectorial addition of $\vec{k}_{inc}$ and $\vec{K}_G$, should terminate on line L to satisfy the phase matching condition. From the diagram, we can see that $\vec{k}_{final}$ indeed terminates on line L at point A. We also note that point B, the intersection point of the

extended grating vector and the solid circle, represents exactly Bragg diffraction. Point A is close to Point B, which means that the ESGC operates near the Bragg diffraction condition [24]. Bragg diffraction acts to suppress other diffraction orders and enforces unidirectional coupling in the ESGC.

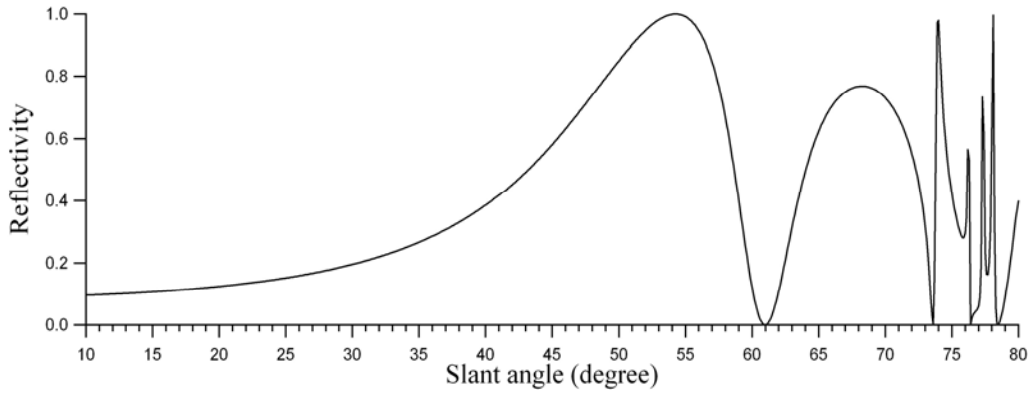

Figure 5.8. The reflectivity of the optimized structure calculated by RCWA.

The excitement of the fundamental leaky mode and the presence of Bragg diffraction should cause abnormal reflection and we should be able to identify the μGA optimized values on the reflection curve as discussed in [53]. To this end, we carried out a detail rigorous coupled wave analysis (RCWA) [27] on the μGA optimized ESGC. Figure 5.8 shows the diffraction efficiency of the zeroth reflected order as a function of the slant angle. It is evident that the optimum slant angle 59.7° is very close to the minimum reflection angle of 61.5°. The small discrepancy is caused by the different source used in the RCWA (plane wave) and FDTD (waveguide mode) simulations. This provides an additional means to verify whether the ESGC design is optimal.

5.2.3 Fabrication and alignment tolerance

We now examine fabrication tolerances for the grating groove width and the slant angle for λ=1.55μm. The grating groove width can be difficult to control during fabrication and we find that a variation of ±18nm relative to the optimized value of 213nm (or ±8.45% change) causes the coupling efficiency to drop to 62.2%. We also find that the coupling efficiency is greater than 63.1% for over a ±3° change in the slant angle. We also simulated the performance of the structure as a function of the misalignment of fiber position along x-direction. Results show that a misalignment less than ±0.7μm is required for the coupling efficiency to be 63.5% or more. One of the interesting features of the design structure similar to SWGC and SLGC is a relaxed fiber alignment tolerance compared to edge coupling. Challenges in fabrication of the ESGC are also anticipated.

5.3 ESGC simulation and design based on polymer waveguide

The embedded slanted grating coupler is also designed and simulated based on the same polymer waveguide materials used in Chapter 4 with a core index of 1.5073 and cladding index of 1.4600. The same fiber with a core size of 8.3μm, core and cladding indices of 1.47 and 1.4647, respectively, and the same grating index of 2 with the same period number of 18 are also used here. The core thickness of the single mode waveguide is selected to be 1.4μm.

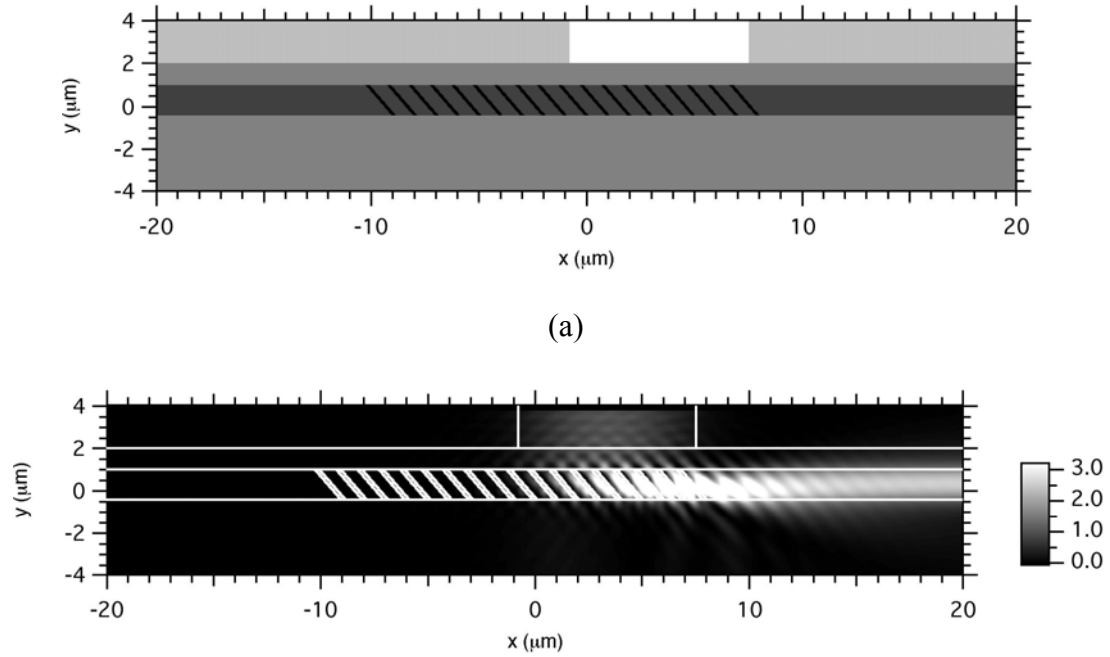

Figure 5.9. (a) Geometry of uniform ESGC based on polymer waveguide optimized by μGA. (b) 2D FDTD result of magnitude squared time averaged E_z component for the uniform ESGC.

Now let's consider a uniform grating coupler which has a uniform fill factor. The μGA FDTD optimized parameters are: Λ=0.6573μm, θ_s=60.35^0 and F_c=3.9μm. The geometry of the design is shown in Figure 5.9(a). Figure 5.9(b) shows the corresponding magnitude squared time averaged E field simulated by FDTD. Notice the smoother mode transition at the grating boundary compared to that with grating on top of the waveguide core as shown in Figure 4.3(b). The input coupling efficiency is about 72.1% (compared to the 66.8% result of the design in Figure 4.3(b)).

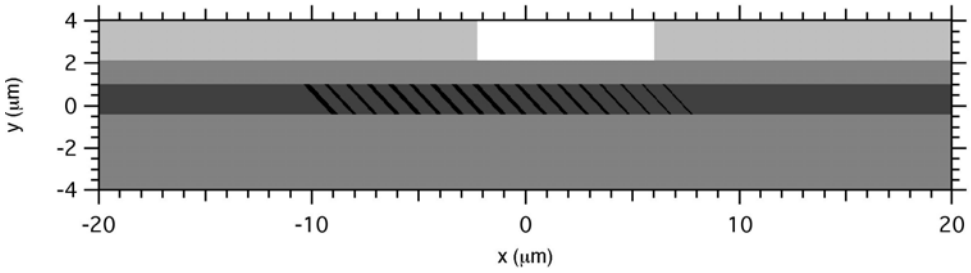

(a)

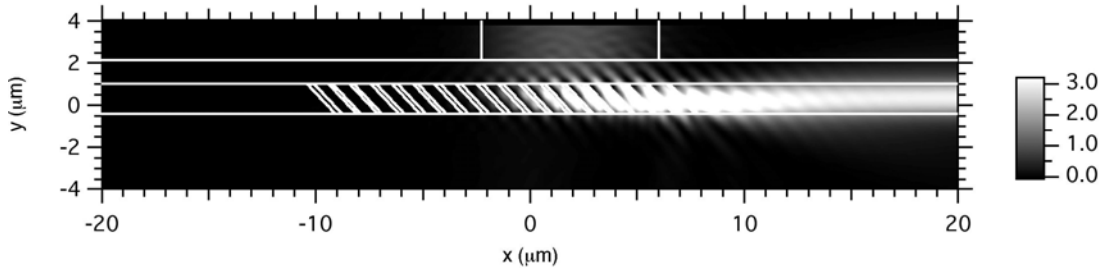

(b)

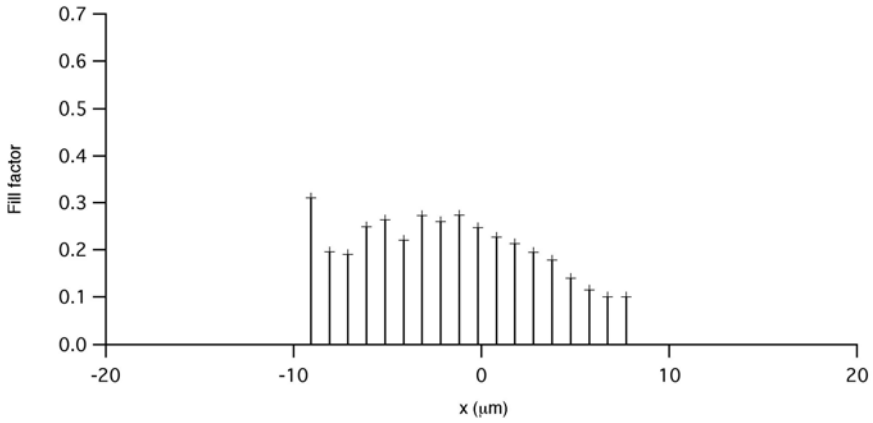

(c)

Figure 5.10. (a) Geometry of non-uniform ESGC based on polymer waveguide optimized by μGA. (b) 2D FDTD result of magnitude squared time averaged E_z component for the non-uniform ESGC. (c) Fill factor distribution of the non-uniform ESGC 2D FDTD result of magnitude squared time averaged E_z in (a).

To further improve the coupling efficiency, the μGA optimized design with non-uniform fill factor is shown in Figure 5.10(a), (b) and (c). The design has Λ=0.6573μm, θ_s=60.35^0, F_c=3.9μm. Now the coupling efficiency is about 83.4% (compared to the result of 80.1% with the grating on top of the waveguide in Figure 4.4(b)).

In the above embedded structure designs, the effective index of the grating area is higher than that of the output waveguide (without grating area) for the high index of the grating material. The effective index difference causes back reflection at the grating boundary when light propagates over it. In order to avoid that, the waveguide core material is replaced by the cladding material with a lower index to lessen the index difference. Therefore higher coupling efficiency is expected.

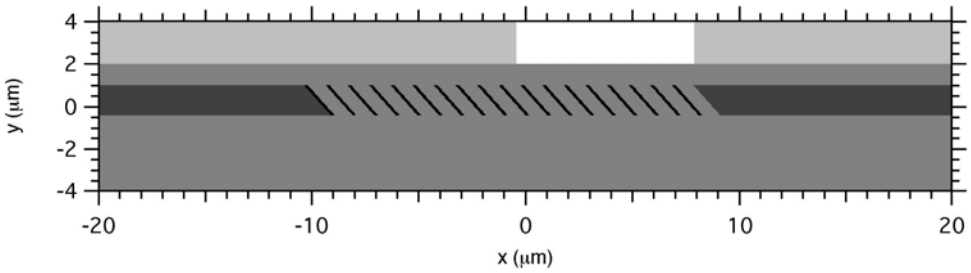

(a)

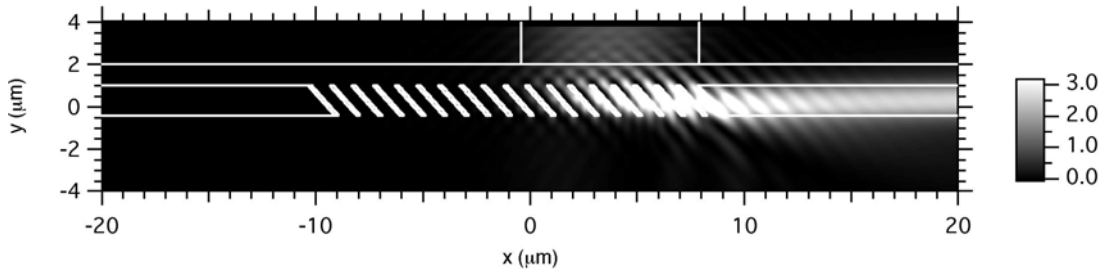

(b)

Figure 5.11. (a) Geometry of uniform ESGC based on polymer waveguide optimized by μGA. (b) 2D FDTD result of the magnitude squared time averaged E_z component for the uniform ESGC.

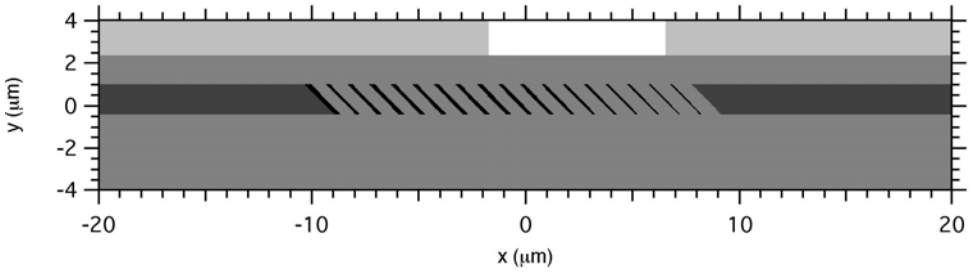

(a)

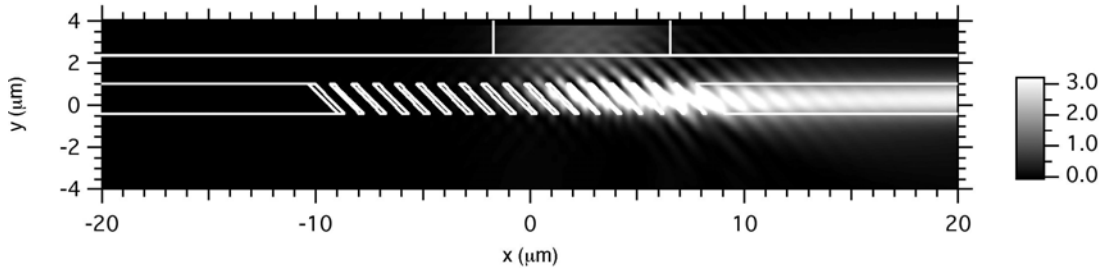

(b)

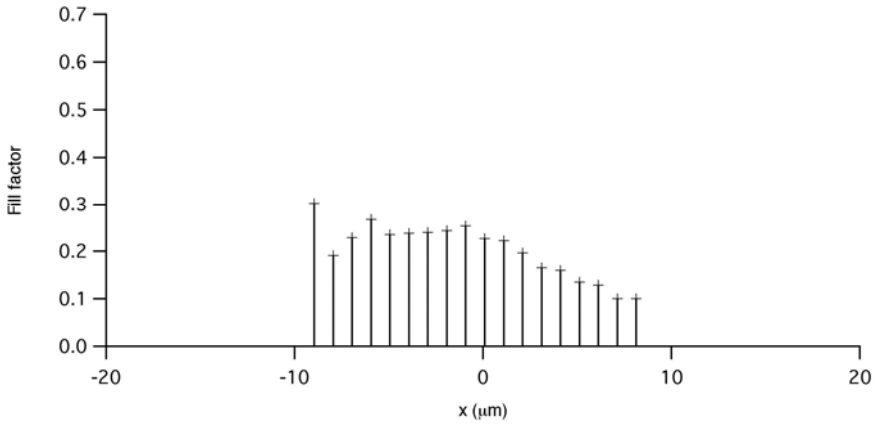

(c)

Figure 5.12. (a) Geometry of non-uniform ESGC based on polymer waveguide optimized by μGA. (b) 2D FDTD result of the magnitude squared time averaged E_z component for the non-uniform ESGC. (c) Fill factor distribution of the the non-uniform ESGC 2D FDTD result of magnitude squared time averaged E_z in (a).

The geometry of the uniform design (Λ=0.6573μm, θ_s=60.35^0 and F_c=3.9μm) is shown in Figure 5.11(a). Figure 5.11(b) shows the corresponding magnitude squared time averaged E field simulated by FDTD. The coupling efficiency is improved to 74.5% now.

Results of the μGA optimized design with non-uniform fill factor are shown in Figure 5.12(a), (b). Figure 5.12(c) shows the distribution of the fill factor along x-direction. The design has Λ=0.6573μm, θ_s=60.35^0, F_c=3.9μm. Now the coupling efficiency is 85.4%.

5.4 Conclusions

The embedded slanted grating structures, in which the grating is moved from the top of the waveguide in SLGC to the waveguide core, are designed and simulated by μGA FDTD code. Simulations are performed on a 240nm thick silicon-on-insulator (SOI) planar waveguide with up to 75.8% coupling efficiency. The k-vector diagram with RCWA mode solver showed that the phase match condition is satisfied and the Bragg condition is slightly off. The abnormal reflection calculated by RCWA provides an additional means for understanding the principles of ESGC. FDTD simulation results are also given, based on the waveguide material simulated in both Chapters 3 and 4, with a core refractive index of n_1= 1.5073 embedded in a cladding with n_2=1.4600 (refractive index contrast Δ=3.1%). ESGCs may have a higher coupling efficiency than SLGC because there is a smoother mode transition from the grating region to the non-grating region and thus scattering loss is reduced at the boundary.

Chapter 6

SYSTEMATIC DESIGN PROCESS FOR UNIFORM SLANTED GRATING COUPLER AT THE BRAGG ANGLE

The powerful design features of μGA for grating couplers having a minimum feature size of the order of a wavelength or smaller has been demonstrated in the previous chapters. With the help of the k-vector and RCWA mode solver, the basic physical characteristics of strong grating couplers have been confirmed—the phase match condition should be satisfied for efficient coupling. For an efficient input/output coupler design, the Bragg condition should also be satisfied, or at least nearly so. The purpose of this chapter is (without the help of μGA) to summarize a general and systematic procedure for designing a uniform slanted grating coupler in the strong coupling regime at the Bragg angle that has acceptable coupling efficiency. The design procedure is illustrated with two specific examples.

6.1 Design process

Since the grating couplers we are interested in operate in the strong coupling regime, the leaky mode is a function of all the grating parameters: grating fill factor, period, and slanted angle, so that analytic determination of the grating period from the

phase match condition is not possible. From this point of view, the design and optimization of strong grating couplers is far more complicated than weak grating couplers. In Chapters 4 and 5, we designed slanted grating couplers and embedded slanted grating couplers with the help of μGA optimization. Although the μGA 2D-FDTD design tool has demonstrated a powerful optimization capability in grating coupler design, there are two main disadvantages to using this method. First, it does not inherently give us intuitive insight into the principles of strong grating couplers due to the built-in random process of μGA and the purely numerical nature of the FDTD simulation. Second, μGA search/optimization is a time-consuming process. For instance, for a uniform embedded slanted grating coupler structure based on the SOI waveguide structure in Chapter 5, a computational area of 30μm×1.5μm with Yee cell size of 10nm×10nm, takes about 14 days for 500 generations to allow μGA fitness function to converge. This is using a parallel μGA with a population size of 5 individuals on a 4-node cluster, each of which uses a PC with a 2.0-GHz CPU and 1.0 GB of RAM.

According to k-vector and RCWA leaky mode analysis of μGA optimized designs, it has been demonstrated that the phase match condition must be closely satisfied. At the same time, if the Bragg diffraction condition is satisfied or very nearly, the design will have high coupling efficiency. Based on this understanding, we developed a general and systematic procedure for designing a uniform slanted grating coupler at the Bragg angle without the help of μGA.

When designing a uniform slanted grating coupler, the waveguide is usually given, which implies that the core index (n_{core}), cladding index ($n_{cladding}$), core thickness

(t) and wavelength (λ) are known. In addition, the grating material (n_g) is also assumed to be known. The grating is embedded into the waveguide core or on top of the waveguide core. At this point, only the grating period along x-direction (Λ), grating slant angle (θ_s) and fill factor (f) need to be determined, which can be accomplished with the following procedure:

1. Select a fill factor for the grating determined by fabrication feasibility (for example, 0.5 or 0.3). Once a fill factor is fixed, the circle in the k-vector diagram is fixed; n_{ave} is determined by the Equation 3.1.

2. Assume the Bragg condition is satisfied. Once a slant angle is selected, the grating period Λ can be calculated directly for normal incidence through the following relationship:

$$L = \frac{\lambda_0}{\Lambda} = \cos(2\theta_s - 90^0) \times n_{ave} . \qquad (7.1)$$

3. Numerically determine the effective index, n, of the mode using RCWA mode solver.

4. Compare the value of L in step2 and n in step 3. Scan different slant angles until a slant angle is found for which L=n.

5. Once the grating structure is fixed (according to the reciprocal relationship between input coupler and output couplers), selection of the fiber and its position can be decided by calculating the field generated by the grating when operated as an output coupler. The number of grating periods can be determined by the width of the fiber as long as the extension of the grating covers the incident beam.

Determine the fiber and its position relative to the grating, F_c (the relative distance between the center of the fiber and the left edge of the grating). A FDTD single- case

simulation is performed on the final structures obtained in the above as output couplers without fiber structure. Select a fiber available commercially to closely match the output beam size. The mode overlap integral between fiber mode and output field with different fiber shifts can determine an appropriate position of the fiber. The output coupling efficiency should be equal to that of the input coupling.

6. The input coupler with final grating and fiber structure is then modeled using the FDTD code to evaluate the performance.

The structure designed could be used either as the final one if it meets the efficiency requirement, or as a good starting point in the next μGA search to save computational time. If the above procedures are not sufficiently effective, we could explore using other values of grating materials and other values of the waveguide thickness t. Generally, a successful strong grating coupler design using the above procedure depends on the specific case.

6.2 Design example based on SOI waveguide

We will use the same SOI waveguide structure and materials of Chapter 5 to illustrate our design approach. The single-mode planar waveguide has a 240nm-thick core layer of Si with refractive index 3.4000 and the lower cladding of SiO_2 has refractive index of 1.4440 and is assumed to be thick enough so that no light is coupled into the Si substrate. The upper cladding is assumed to have a refractive index of 1.4600. The grating material is the same as the upper cladding.

6.2.1 Fill factor of 0.328

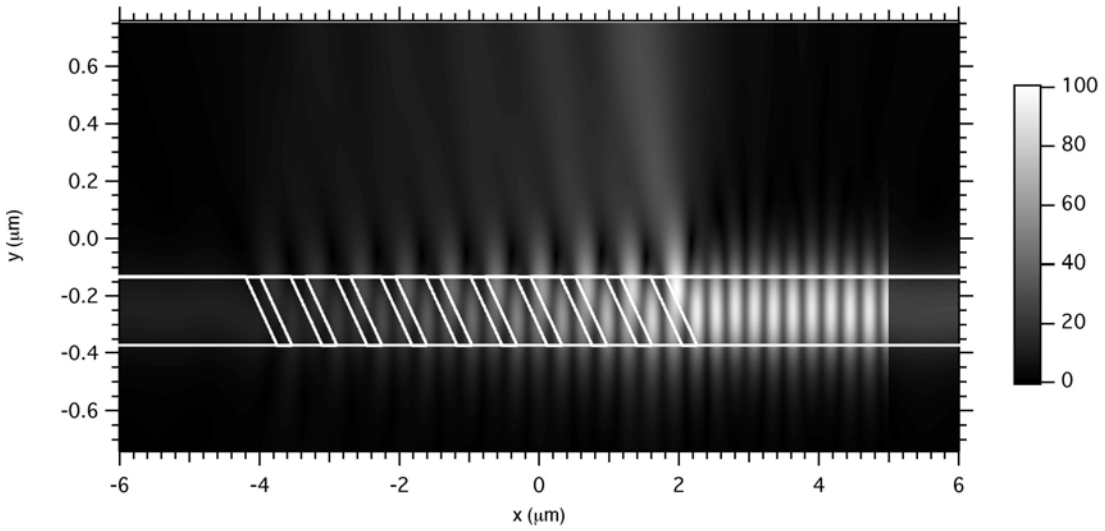

Figure 6.1. 2D FDTD result of the magnitude time averaged E_z component of output coupler.

First we will select the fill factor which we set equal to the one obtained by μGA in Chapter 5, f=0.328. Now we use the RCWA mode solver code to search the Bragg angle. It is found to be 62.05^0 with L=n=2.4099 which means the phase match and Bragg conditions are satisfied at the same time, and the corresponding Λ is 0.6433μm. With these grating structure parameters, the FDTD simulation is run with the grating structure as an output coupler. Figure 6.1 shows the magnitude time averaged E_z field. As seen in Figure 6.1, a guide mode is launched from the right side and propagates towards the grating. The light is eventually coupled out traveling upwards. The number of the periods is selected to be 10 here to allow most of the light to be coupled out. Figure 6.2(a) shows the cross section of the near field pattern in Figure 6.1. A typical Erbium-doped optical fiber, with a core size of 4.4 μm and core and cladding indices of 1.4840 and 1.4600,

respectively, is used. The field profile of the fiber mode is shown in Figure 6.2(b). The same fiber mode will be used also for different fill factor designs later. The output coupling efficiency calculated using the mode overlap integral shows that coupling efficiency is 63.2%~67.6% when Fc is 4.07μm~4.67μm. The optimum coupling efficiency occurs for Fc=4.67μm.

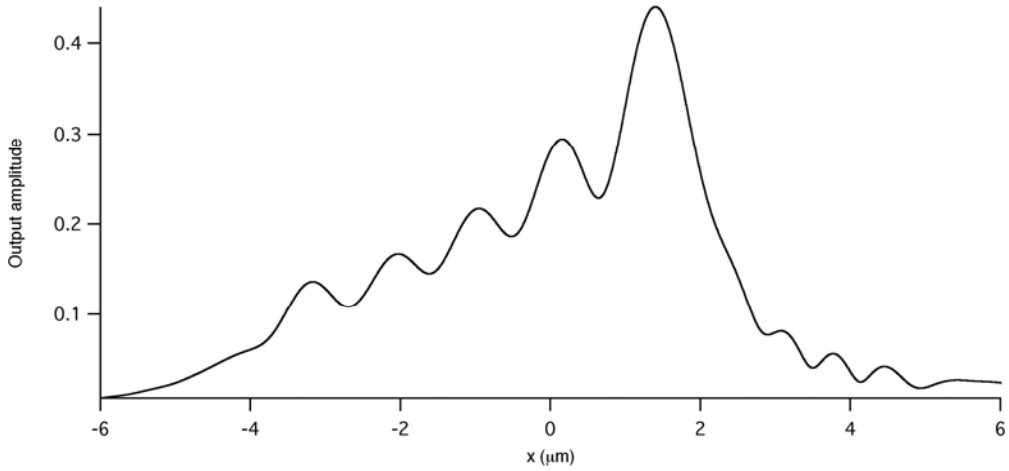

(a)

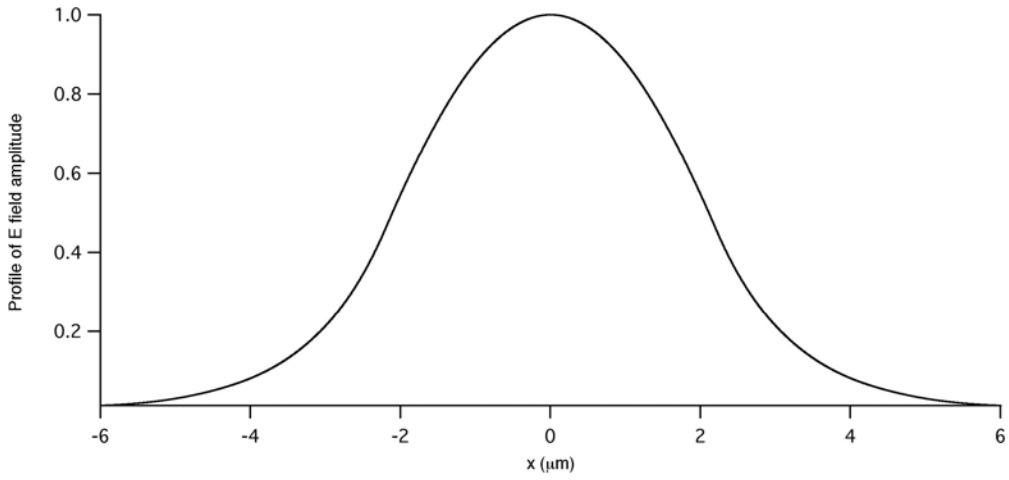

(b)

Figure 6.2. (a) Cross section of the near field pattern of Figure 6.1. (b) Cross section of the fiber mode.

Finally, an FDTD simulation is run on the structure operating as an input coupler to evaluate the input coupling efficiency (shown as the magnitude squared time averaged E_z component in Figure 6.3). The input coupling efficiency is 68.6% which is very close to the corresponding output coupling efficiency. Notice that the μGA optimized result with a fill factor of 0.328 is 69.8%.

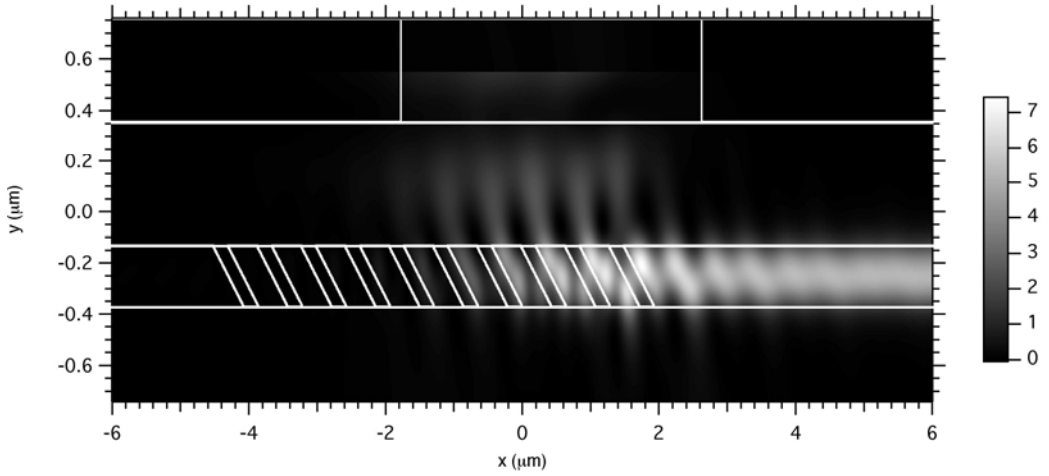

Figure 6.3. 2D FDTD result of magnitude squared time averaged Ez component of input coupler with f=0.328.

6.2.2 Fill factor of 0.5

Following the same procedure, a grating coupler with a fill factor of 0.5 is designed as follows. With the aid of RCWA mode solver, the "critical" point that satisfies the phase match and Bragg condition is the one with a slant angle=62.5º and Λ=0.723μm. As an output coupler with 10 periods, and the above grating structural parameters, a single FDTD run is performed. The simulation result of the magnitude time averaged E_z component and the profile of the corresponding output beam are shown in Figure 6.4(a) and (b), respectively. The output coupling efficiency with mode overlap

shows that, when F_c is 5.39μm, the output coupling efficiency is about 57.8%. Now as an input coupler, the FDTD simulation is run and simulation results are shown in Figure 6.5 with the magnitude squared time averaged E_z component. Compared to the μGA optimized result of 62.1% with a fixed fill factor of 0.5, the input coupling after mode overlap integral calculation is 58.9%.

For the design of a slanted grating coupler in which the grating is positioned on top of grating, the thickness of the grating has to be selected before using the procedure described here.

μGA always tries to find the best result that could balance all the factors (phase match, Bragg condition and fiber mode) affecting the coupling efficiency. For instance, in some cases, the Bragg condition has to be a little bit off to balance the overall efficiency if the fiber mode cannot be matched well. However, for a good design, the Bragg condition should be satisfied more stringently. That is the basis on which the above procedure works.

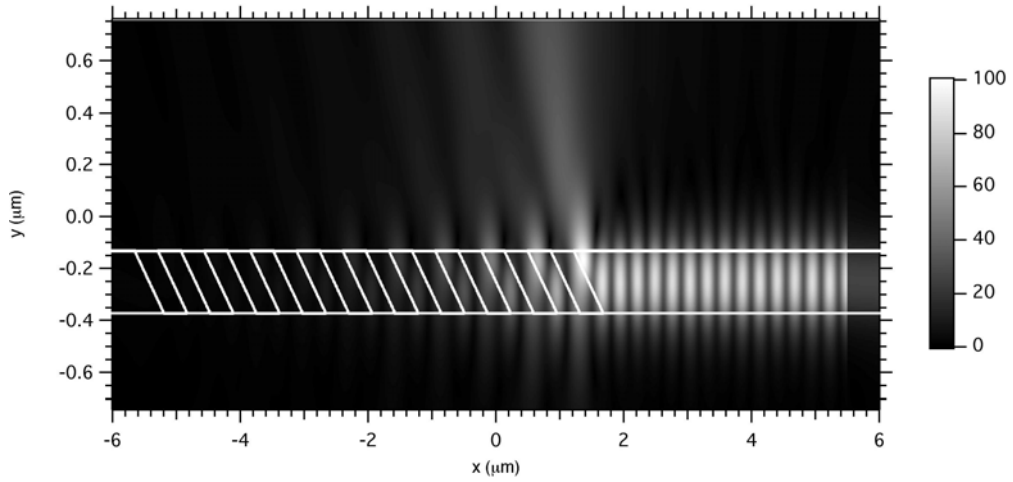

(a)

Figure 6.4. (a) 2D FDTD result of magnitude time averaged E_z component for the output coupler.

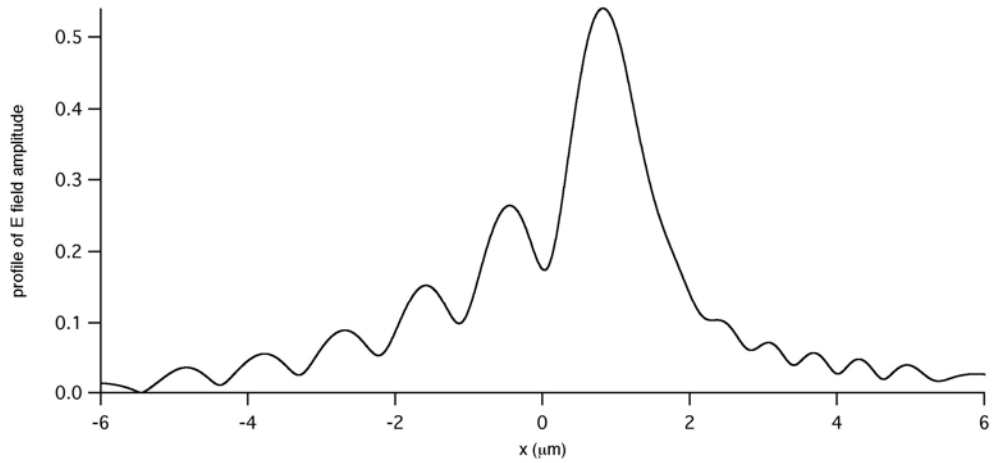

(b)

Figure 6.4. Continue (b) Cross section of the near field pattern in (a).

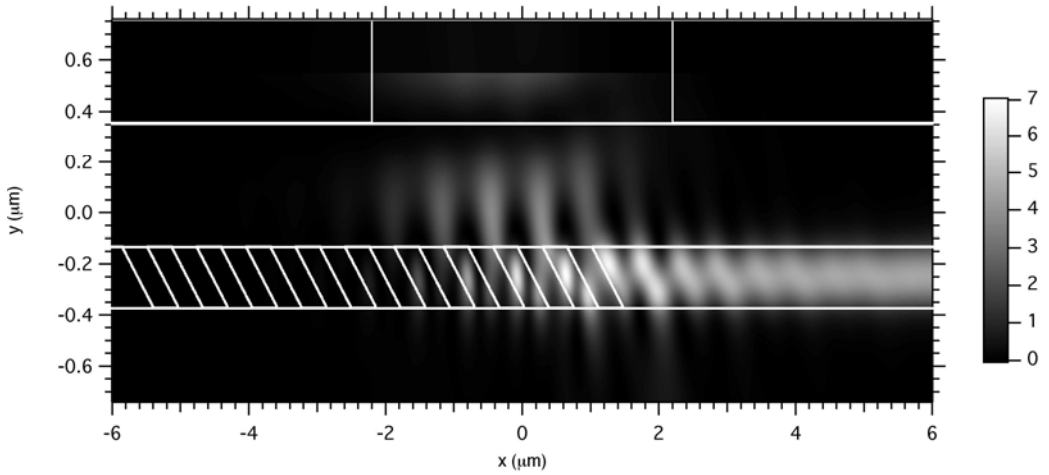

Figure 6.5. 2D FDTD result of magnitude squared time averaged Ez component of input coupler with f=0.5.

6.3 Conclusions

Without the aid of μGA optimization, a systematic design procedure for the uniform slanted grating coupler is developed in this chapter based on the physical understanding of slanted grating couplers in the strong coupling regime. A specific design for a SOI waveguide is given using this procedure, which turns out not only to prove the effectiveness of our design procedure, but also confirms that our analysis and physical understanding of the grating coupler in the strong coupling regime using a k-vector diagram with RCWA mode solver is correct.

Chapter 7

DISCUSSION AND CONCLUSIONS

This dissertation focuses on the design and simulation of compact grating couplers in the strong coupling regime for vertical fiber coupling into a single mode fiber. With the design and optimization function of μGA FDTD, three types of grating couplers: stratified grating coupler (SWGC), slanted grating coupler and embedded grating coupler have been designed as original methods for different high index contrast waveguides. K-vector diagrams with RCWA mode solver methods have been explored in order to understand the physical principles of the designed structures. Although the μGA FDTD code has powerful design and optimization functions in designing grating couplers with minimum feature size of the order of a wavelength or smaller, the procedure is time consuming and computationally intense. Therefore a systematic design procedure for uniformly slanted grating couplers at the Bragg angle was developed and was proven effective. Coupling light from fibers to high index contrast waveguides is a basic and important, but difficult function in integrated optics. Future recommended research is given after the summary of the dissertation work.

7.1 Summary

After the research background and computation tools are introduced in Chapter 2, a compact stratified grating coupler was designed for vertical fiber coupling into high

index contrast waveguide and was presented in Chapter 3. The SWGC consists of three binary grating layers embedded in the waveguide upper cladding with the bottom-most layer situated on top of the waveguide core. Since the layers in the SWGC are fabricated sequentially, the binary grating layers can be laterally shifted relative to one another to create a stratified grating structure analogous to a volume grating with slanted fringes. A grating with maximum first order efficiency at normal incidence can be achieved using this technique. The large index difference between the grating material and the cladding (0.3 to 2.0) strengthens the coupling effect, such that short grating lengths (10-20μm) comparable to the mode field diameter of a fiber are sufficient for high efficiency coupling. One μGA FDTD designed and optimized result with an input coupling efficiency of ~72% is given.

From a RCWA mode solver and k-vector diagram analysis, the phase-matching condition and Bragg condition are satisfied simultaneously with respect to the fundamental leaky mode supported by the optimized SWGC. Further FDTD simulation performed on the optimized design shows that the SWGC design has a relatively broad spectral response and much greater fiber misalignment tolerance than traditional pigtailing coupling. A lateral shift of ±3μm results in less than 1 dB of additional coupling loss. A similar result has been found for the other two types of strong grating couplers considered in this dissertation. From a tolerance analysis, the fabrication tolerance is reasonable but fabrication challenges are still anticipated.

Single layer slanted grating couplers (SLGC's) that operate in the strong coupling regime with a parallelogramic-shaped profile were discussed in Chapter 4. We were originally motivated to examine such structures by the development of a new etching

technique that readily achieves slanted etches and avoids the complicated alignment procedure in SWGC. With the help of μGA 2-D FDTD, a high efficiency (~66.8%) SLGC with a uniform fill factor has been designed. In order to further improve the efficiency, a non-uniform SLGC with a gradual change of fill factors has also been designed with a coupling efficiency of 80.1%. Reciprocal relationship has been found in strong grating couplers, i.e., any grating designed to serve as an input coupler can be also used as an output coupler. Using this, analysis of an output coupler may give us more insight into the mechanism of an input coupler and non-uniform input coupler. In addition, with the RCWA mode solver and k-vector diagram analysis, it was found that the phase-matching condition and Bragg condition are satisfied simultaneously with respect to the fundamental leaky mode in both the optimized uniform and non-uniform SLGC. Broad spectral response and relaxed fiber misalignment tolerance was found for the SLGC structure, too. The criterion for the tolerance is the coupling efficiency being maintained greater than 60%. It is interesting that the tolerance for the slant angle is ±4° which is more relaxed than for the weak grating coupler.

The third type of strong grating couplers, the embedded slanted grating structure, where the grating is moved from the top of waveguide in SLGC to the waveguide core, is designed and simulated in Chapter 5. It is especially suitable for a high index contrast waveguide like SOI where light is strongly confined in a waveguide core layer of a few hundred nanometers in the transverse dimension. The field distribution in the grating region of the ESGC is centered within the waveguide, which improves the mode transition from the grating region to the non-grating region and thus reduces scattering loss at the boundary. Simulations were performed on 240nm thick silicon-on-insulator

(SOI) planar waveguide with up to 75.8% coupling efficiency. K-vector diagrams with the RCWA mode solver proved that the phase match condition is satisfied with the Bragg condition a little bit off to balance the overall efficiency (if the fiber mode cannot be matched well). There is also broad spectral response and relaxed fiber misalignment tolerances in ESGC. Tolerance analysis anticipates the fabrication challenges for high efficiency. In addition to the SOI waveguide design, we applied ESGC to waveguides with the same waveguide materials as in Chapters 3 and 4. A coupling efficiency of up to 85.4% is possible because of the smoother mode transition at the grating boundary.

A systematic design procedure for uniform slanted grating coupler was developed in chapter 6 based on the physical understanding of slanted grating couplers in the strong coupling regime. A specific design for a SOI waveguide proved the effectiveness of this procedure. Our analysis and physical understanding of grating couplers in the strong coupling regime using a k-vector diagram with RCWA mode solver is correct.

7.2 Future research

Coupling structures between an optical fiber and a high index contrast waveguide are fundamental components and have been a standing challenge in integrated optics. In an effort to move this important issue along, this dissertation work mainly concentrates on the 2-D numerical design and analysis of strong grating couplers. The results presented show the promise of our methods, especially in applications involving integrated optics sensors where fiber-to-chip coupling can be lossy because there is a difference of five or six orders of magnitude between the incoming power and the detected power in the end. The next recommended efforts may focus on (1) 3-D FDTD

evaluation of the 2-D structures presented in this dissertation, and (2) fabrication of stratified grating coupler and slanted grating coupler structures.

7.2.1 3-D analysis and evaluation

An important next step in evaluating the properties of the design is to extend the 2-D results presented in this dissertation to a 3-D analysis. 3-D FDTD code has been developed for air trench bend design [45] in our group, which needs to be modified for grating coupler applications. We expect that the grating ridge on top of a broad waveguide will need to be semicircular to focus the light into the lateral waveguide which has to be gradually tapered into a single channel waveguide.

7.2.2 Fabrication of stratified and slanted grating structures

Fabrication of a stratified grating requires planarizing homogeneous layers over binary gratings and aligning subsequent grating layers at specific offset distances. A free space stratified grating has been successfully fabricated using standard microfabrication techniques in Dr. Chamber's dissertation work [42] [58]. It is anticipated that more careful management of the fabrication tolerance, especially of the grating alignment, will be necessary for the successful fabrication of high efficiency SWGC. Electron beam lithography can be used for precise patterning and alignment.

As an initial investigation for fabricating high aspect ratio slanted grating structures, a polymer slanted grating can be fabricated using Oxygen Atomic Etching (OAE) techniques being developed at Los Alamos National Laboratory and cooperation with us is ongoing. Future research is also needed to develop slanted gratings using

electron beam lithography and reactive ion etching (RIE) which are being facilitated in our center at UAH.

REFERENCES

[1] J. D. Joannopoulos, R. D. Meade, and J. N. Winn, *Photonic Crystals: Molding the Flow of Light*, (Princeton University Press, Princeton, N.J., 1995).

[2] J. D. Joannopoulos, P. R. Villeneuve, and S. Fan, "Photonic crystals: Putting a new twist on light," Nature, Vol. 386, pp. 143-149, 1997.

[3] Y. Hibino, "High contrast waveguide devices," Conf. Opt. Fiber Commun. Tech. Dig. Ser., Vol. 54, pp. WB1/1-WB1/3, 2001.

[4] Manolatou, S. G. Johnson, S. Fan, P. R. Villeneuve, H.A.Haus, and J.D. Joannopoulos, "High-density integrated optics," J. Lightwave Technol., Vol. 17, pp. 1682-1692, 1999.

[5] B. Mersali, A. Ramdane, and A. Carenco, "Optical-mode transformer: A III-V circuit integration enabler," IEEE J. Quantum Electron., Vol. 3, pp. 1321-1331, 1997.

[6] I. Moerman, P. P Van Daele, and P.M. Demeester, "A review on fabrication technologies for the monolithic integration of tapers with III-V semiconductor devices," IEEE J. Quantum Electron., Vol. 3, pp. 1308-1320, 1997.

[7] P.V. Studenkov, M.R. Gokhale, and S.R. Forrest, "Efficient coupling in integrated Twin-waveguide lasers using waveguide tapers," IEEE Photon. Technol. Lett., Vol. 11, pp. 1096-1098, 1999.

[8] V. R. Almeida, R. R. Panepucci, and M. Lipson, "Nano-taper for compact mode conversion," Opt. Lett., Vol. 28, pp.1302-1304, 2003.

[9] T. Tamir, *Integrated Optics*, (Springer Verlag, 1975).

[10] R.Ulrich, "Efficiency of optical-grating couplers," J. Opt. Soc. Am., Vol. 63, pp. 1419-1431, 1973.

[11] T.Tamir and S. T. Peng, "Analysis and design of grating couplers," Appl. Phys., Vol. 14, pp. 235-254, 1977.

[12] R. Waldhäusl, B. Schnabel, P. Dannberg, E. Kley, A. Bräuer, and W. Karthe, "Efficient coupling into polymer waveguide by gratings," Appl. Opt., Vol. 36, pp. 9383-9390, 1997.

[13] V. A. Sychugov, A. V. Tishchenko, B. A. Usievich, and O. Parriaux, "Optimization and control of grating coupling to or from a Silicon-based optical waveguide," Opt. Eng., Vol. 35, pp. 3092-3100, 1996.

[14] J. C. Brazas, and L. Li, “Analysis of input-grating coupler having finite lengths,” Appl. Opt., Vol. 34, pp. 3786-3792, 1995.

[15] R. W. Ziolkowski, and T. Liang, “Design and characterization of a grating-assisted coupler enhanced by a photonic-band-gap structure for effective wavelength-division multiplexing,” Opt. Lett., Vol. 22, pp. 1033-1035, 1997.

[16] D. Pascal, R. Orobtchouk, A. Layadi, A. Koster, and S. Laval, “Optimized coupling of a gaussian beam into an optical waveguide with a grating coupler: Comparison of experimental and theoretical results,” Appl. Opt., Vol. 36, pp. 2443-2447, 1997.

[17] T. W. Ang, G. T. Reed, A. Vonsovici, A. G. R. Evans, P. R. Routley, and M. R. Josey, “Effects of grating heights on highly efficient unibond SOI waveguide grating couplers,” IEEE Photon. Technol. Lett., Vol. 12, pp. 59-61, 2000.

[18] S. M. Schultz, E. N. Glytsis, and T. K. Gaylord, “Volume grating preferential-order focusing waveguide coupler,” Opt. Lett., Vol. 24, pp. 1708-1710, 1999.

[19] S. M. Schultz, E. N. Glytsis, and T. K. Gaylord, “Design of a high-efficiency volume grating coupler for line focusing,” Appl. Opt. Vol. 37, pp. 2278-2287, 1998.

[20] S.-D. Wu and E. N. Glytsis, "Volume holographic grating couplers: Rigorous analysis by use of the finite-difference frequency-domain method," Appl. Opt. Vol. 43, pp. 1009-1023, 2004.

[21] J. K. Bulter, S. Nai-Hsiang, G. A. Evans, L. Pang, and P. Congdon, "Grating-assisted coupling of light between semiconductor glass waveguides," IEEE J. Lightwave Technol., Vol. 16, pp. 1038-1040, 1998.

[22] R. Orobtchouk, A. Layadi, H. Gualous, D. Pascal, A. Koster, and S. Laval, “High-efficiency light coupling in a submicrometric silicon-on-insulator waveguide,” Appl. Opt., Vol. 39, pp. 5773-5777, 2000.

[23] G. Z. Masanovic, V. M. N. Passaro, and T. R. Graham, "Dual grating-assisted directional coupling between fibers and thin semiconductor waveguides," IEEE Photon. Technol. Lett., Vol. 15, pp. 1395-1397, 2003.

[24] H. Kogelnik and T.P.Sosnowski, “Holographic thin film couplers,” Bell Syst. Tech. J., Vol. 49, pp. 1602-1608, 1970.

[25] O. Parriaux, V. A. Sychugov, and A. V. Tishchenko, “Coupling gratings as waveguide functional elements,” Pure Appl. Opt., Vol. 5, pp. 453-469, 1996.

[26] D. Taillaert, W. Bogaerts, P. Bienstman, T. F. Krauss, P. Van Daele, I. Moerman, S. Verstuyft, K. Mesel, and R. Baets, “An out-of-plane grating coupler for efficient butt-coupling between compact planar waveguides and single-mode fibers,” IEEE J. Quantum Electron., Vol. 38, pp. 949-955, 2002.

[27] M. G. Moharam and T. K. Gaylord, “Diffraction analysis of dielectric surface-relief gratings,” J. Opt. Soc. Am. Vol. 72, pp. 1385-1392, 1982.

[28] A. Taflove, *Computational Electrodynamics: The Finite-Difference Time-Domain Method*, (Artech House, Massachusetts, 1995).

[29] J. Jiang, J. Cai, G. P. Nordin, and L. Li, "Parallel micro-genetic algorithm design of photonic crystal and waveguide structures," Opt. Lett., Vol. 28, pp. 2381-2383, 2003.

[30] J. Jiang, *Rigorous Analysis and Design of Diffraction Optical Elements*, PhD dissertation, University of Alabama at Huntsville, 2000.

[31] J. P. Berenger, "A perfectly matched layer for the absorption of electromagnetic waves," J. Comput. Phys., Vol. 114, pp. 185-200, 1994.

[32] K. Krishnakumar, "Micro-genetic algorithm for stationary and non-stationary function optimization," SPIE, Vol. 1196, pp. 289-296, 1989.

[33] Z. Michalewicz, *Genetic Algorithm + Data Structures + Evolution Programs*, (Springer-Verlag, Berlin, 1992).

[34] D. E. Goldberg, *Genetic Algorithm in Search, Optimization, and Machine Learning*, (Addison Wesley, Massachusetts, 1989).

[35] S. Kim, G. P. Nordin, J. Jiang, and J. Cai, "Micro-genetic algorithm design of hybrid conventional waveguide and photonic crystal structures," Opt. Eng., Vol. 43, pp. 2143-2149, 2004.

[36] J. Jiang and G. P. Nordin, "A Rigorous Unidirectional Method for Designing Finite Aperture Diffractive Optical Elements," Opt. Express, Vol. 7, pp. 237-242, 2000.

[37] L. Li, G. P. Nordin, J. M. English, and J. Jiang, "Small-area bends and beamsplitters for low index-contrast waveguides," Opt. Express, Vol. 11, pp. 282-290, 2003.

[38] R. Petit, *Electromagnetic Theory of Gratings*, (Springer-Verlag, Berlin, 1980).

[39] K. C. Chang, V. Shah, and T. Tamir, "Scattering and guiding of waves by dielectric gratings with arbitrary profiles," J. Opt. Soc. Am., Vol. 70, pp. 804-813, 1980.

[40] W. H. Press, S. A. Teukolsky, W. T. Vetterling, and B. P. Flannery, *Numerical Recipes in Fortran 90*, (Cambridge University Press, 1996).

[41] D. M. Chambers, and G. P. Nordin, "Stratified volume diffractive optical elements as high-efficiency gratings," J. Opt. Soc. Am. A/Vol. 5**,** pp. 1184-1193, 1999.

[42] D. M. Chambers, G. P. Nordin, and S. Kim, "Fabrication and analysis of a three-layer stratified volume diffractive optical element high-efficiency grating," Opt. Express, Vol. 11, pp. 27-38, 2003.

[43] B. Wang, J. Jiang, D. M. Chambers, J. Cai, and G. P. Nordin, "Stratified waveguide grating coupler for normal fiber incidence," Opt. Lett., Vol.30, pp. 3316-3323, 2005.

[44] R. Syms, and J.Cozens, *Optical Guided Waves and Devices*, chapter 6 and 9, (McGraw-Hill, New York, 1992).

[45] L. Xia, *Compact Waveguide Bends and Application in a Waveguide Depolarizer*, PhD dissertation, University of Alabama at Huntsville, 2004.

[46] W. Streifer, R. Burnham, and D. Scifres, "Analysis of grating-coupled radiation in GaAs:GaAlAs lasers and waveguides--II: Blazing effects," IEEE J. Quantum Electron., Vol. 12, pp. 494–499, 1976.

[47] W. Streifer, D. Scifres, and R. Burnham, "Analysis of grating-coupled radiation in GaAs:GaAlAs lasers and waveguides," IEEE J. Quantum Electron., Vol. 12, pp. 422–428, 1976.

[48] B. Wang, J. Jiang, and G. P. Nordin, "Compact slanted grating couplers for vertical coupling between fibers and planar waveguides," Opt. Express, Vol. 12, pp. 3313-3326, 2004.

[49] M. Matsumoto, "Analysis of the blazing effect in second-order gratings," IEEE J. Quantum Electron., Vol. 28, pp. 2016-2023, 1992.

[50] M. Li, and S. J. Sheard, "Experimental study of waveguide grating couplers with parallelogramic tooth profiles," Opt. Eng., Vol. 35, pp. 3101-3106, 1996.

[51] T. Liao, S. Sheard, M. Li, J. Zhuo, and P. Prewett, "High-efficiency focusing waveguide grating coupler with parallelogramic groove profiles," IEEE J. Lightwave Technol., Vol.15, pp. 1142-1148 ,1997.

[52] M. Li, and S. J. Sheard, "Waveguide couplers using parallelogramic-shaped blazed gratings," Opt. Commun., Vol. 109, pp. 239-245, 1994.

[53] A. V. Tishchenko, N. M. Lyndin, S. M. Loktev, V. A. Sychugov, and B. A. Usievich, "Unidirectional waveguide grating coupler by means of parallelogramic grooves," SPIE, Vol. 3099, pp. 269-277, 1997.

[54] J. Michael Miller, Nicole de Beaucoudrey, Pierre Chavel, Jari Turunen, and Edmond Cambril, "Design and fabrication of binary slanted surface-relief gratings for a planar optical interconnection," Appl. Opt., Vol. 36, pp. 5717-5727, 1997.

[55] Personal communications with Dr. Mark Hoffbauer in Los Alamos National Laboratory about slant etches using atomic oxygen technique.

[56] R.Ulrich, "Optimum excitation of optical surface waves," J. Opt. Soc. Am. Vol. 61, pp. 1467-1477, 1971.

[57] L. C. West, C. Roberts, J. Dunkel, G. Wojcik, and J. Mould, Jr., "Non uniform grating couplers for coupling of Gaussian beams to compact waveguides," Integrated Photonics Research Technical Digest, Optical Society of America, 1994.

[58] D. M. Chambers, *Stratified Volume Diffractive Optical Elements*, PhD dissertation, University of Alabama at Huntsville, 2000.